Rain-on-snow responses to a warmer Pyrenees: a sensitivity analysis using a physically-based hydrological model

Josep Bonsoms [1], Juan I. López-Moreno [2], Esteban Alonso-González [3], César Deschamps-Berger [2], Marc Oliva [1]

[1] Department of Geography, Universitat de Barcelona, Barcelona, Spain

[2] Instituto Pirenaico de Ecología (IPE-CSIC), Campus de Aula Dei, Zaragoza, Spain

[3] Centre d'Etudes Spatiales de la Biosphère (CESBIO), Université de Toulouse, CNES/CNRS/IRD/UPS, Toulouse, France.

Corresponding author: Juan I. López-Moreno (nlopez@ipe.csic.es)

Abstract. Climate warming is changing the magnitude, timing, and spatial patterns of mountain snowpacks. A warmer atmosphere may also lead to precipitation phase shifts, with decreased snowfall fraction (Sf). The combination of Sf and snowpack decreases directly affects the frequency and intensity of rain-on-snow (ROS) events, a common cause of flash-flood events in snow dominated regions. In this work we examine the ROS patterns and sensitivity to temperature and precipitation change in the Pyrenees modelling through a physical-based snow model forced with reanalysis climate data perturbed ~~following~~ using a range of values of temperature and precipitation consistent with 21st century climate projections~~ for this mountain range~~. ROS patterns are characteri~~t~~zed by their frequency, rainfall quantity and snow ablation. The highest ROS frequency for the ~~baseline climate period~~historical climate period (1980 – 2019) are found in South-West high-elevations sectors of the Pyrenees (17 days/year). Maximum ROS rainfall amount is detected in South-East mid-elevations areas (45 mm/day, autumn), whereas the highest ROS ablation is found in North-West high-elevations zones (- 10 cm/day, summer). When air temperature is increased from 1ºC to 4ºC with respect to the ~~baseline climate period~~historical climate period, ROS rainfall amount and frequency increase at a constant rate during winter and early spring for all elevation zones. For the rest of the seasons, non-linear responses of the ROS frequency and ablation to warming are found. Overall, ROS frequency decreases in the shoulders of the season across eastern low-elevated zones due to snow cover depletion. However, ROS increases in cold, high-elevated zones where long-lasting snow cover exists until late spring. Similarly, warming induces greater ~~triggers fast~~ ROS ablation (+ 10% per ºC) during the coldest months of the season, high-elevations, and northern sectors where the deepest snow depths are found. On the contrary, small differences in ROS ablation are found for warm and marginal snowpacks. These results highlight the different ROS responses to warming across the mountain range, suggest similar ROS sensitivities in near mid-latitude zones, and will help anticipate future ROS impacts in hydrological, environmental, and socioeconomic mountain systems.

Keywords: Snow, Rain-on-snow, Climate warming, Snow sensitivity, Mountain snowpack, Pyrenees.

Con formato: Inglés (Estados Unidos)

Con formato: Inglés (Estados Unidos)

Con formato: Inglés (Estados Unidos)

Con formato: Inglés (Estados Unidos)

1 Introduction

Mountain snowpacks supply large hydrological resources to the lowlands (García-Ruiz et al., 2015; Viviroli et al., 2011), with important implications in the ecological (Wipf and Rixen, 2010), hydrological (Barnett, 2005; Immerzeel et al., 2020) and socioeconomic systems by providing hydroelectricity (Beniston et al., 2018) or guaranteeing winter tourism activities (Spandre et al., 2019). Climate warming, however, is modifying mountain snowfall patterns (IPCC, 2022), through temperature-induced precipitation changes from snowfall to rainfall (Lynn et al., 2020), leading in some cases to rain-on-snow (ROS) events ~~-~~in snow covered areas where it did not occur before. The upward high-latitude temperature and precipitation trends (Bintanja and Andry, 2017) and warming in mountain regions (Pepin et al., 2022) will likely change future ROS frequency in snow-dominated areas (López-Moreno et al., 2021). ~~. To date, research has been focused on the ROS predictability (Corripio and López-Moreno, 2017), detection and validation methods through remote sensing (Bartsch et al., 2010) and models (Serreze et al., 2021). Several works have examined ROSfrequency from the climatological point of view, by analyzing ROS spatial-temporal patterns for Alaska (Crawford et al., 2020), Japan (Ohba and Kawase, 2020), Norway (Pall et al., 2019; Mooney and Li, 2021) or the Iberian Peninsula mountains (Morán-Tejeda et al., 2019). ROS events have also been linked with Northern Hemisphere and Arctic low-frequency climate modes of variability (Rennert et al., 2009; Cohen et al., 2015) as well as synoptic weather types (Ohba and Kawase, 2020). Further, several works in mountain catchments of Switzerland (Würzer et al., 2016), Germany (Garvelmann et al., 2014a), United States (Marks et al., 1992), Canadian Rockies (Pomeroy et al., 2016) or Spain (Corripio and López-Moreno, 2017), have portioned the contribution of Surface Energy Balance (SEB) components during ROS events.~~ ROS has relevant impacts in the ecosystem. ~~alters snow and soil conditions, since t~~The liquid water percolation in the snowpack due to a ROS event creates ice layers and could alter ~~the snowpack~~its ~~-~~stability (Rennert et al., 2009). In severe ROS events, water percolation reaches the ground, and the subsequent water freezing causes latent heat releases, leading to soil and permafrost warming (Westermann et al., 2011). Positive heat fluxes during ROS events enhance snow runoff (Corripio and López-Moreno, 2017), especially in warm and wet snowpacks (Würzer et al., 2016). ROS can also trigger a snow avalanche in mountain zones (Conway and Raymond, 1993), flash flood events (Surfleet and Tullos, 2013), impacts in tundra ecosystems (Hansen et al., 2014~~3~~) and herbivore populations ~~such as reindeers~~ (Kohler and Aanes, 2004).

Different ROS frequency trends have been found since the last half of the 20st century. In the western United-States and from 1949 to 2003 (Mccabe et al., 2007) found a general ROS frequency decrease in 1500 m ~~-~~but an increase in high elevations. Similarly, the analysis of six major German basins from 1990 to 2011, reveals an upward (downward) ROS frequency trend during winter (spring) at 1500 m and high elevations (Freudiger et al., 2014). On the contrary, from 1979 to 2014, no winter ROS frequency trends were found across the entire Northern-Hemisphere (Cohen et al., 2015). ROS projections for the end of the 21st century suggest a general ROS frequency increase in cold regions and high elevated zones (IPCC, 2019). This is projected for Alaska (Bieniek et al., 2018), Norway (Mooney and Li, 2021), western United-States (Musselman et al., 2018),

Con formato: Inglés (Estados Unidos)

Con formato: Fuente: (Predeterminada) Times New Roman, 11 pto

Con formato: Inglés (Estados Unidos)

Con formato: Inglés (Estados Unidos)

Con formato: Inglés (Estados Unidos)

Con formato: Inglés (Estados Unidos)

Con formato: Inglés (Estados Unidos)

Canada (il Jeong and Sushama, 2018) or Japan (Ohba and Kawase, 2020). In European mid-latitude mountain ranges, such as the Alps, ROS frequency is expected to increase (decrease) in high (low) elevation sectors (Beniston and Stoffel, 2016; Morán-Tejeda et al., 2016). López-Moreno et al. (2021) compared the ROS sensitivity to climate warming across 40 global basins and detected the highest ROS frequency decreases in low-elevated and warm Mediterranean mountain sites. Despite the increasing understanding of ROS spatio-temporal past and future trends, little is known about the ROS sensitivity to climate warming across southern European mountain ranges, such as the Pyrenees.

Here we examine the ROS sensitivity to temperature and precipitation change for low (1500 m), mid (1800 m) and high (2400 m) elevations of the Pyrenees. ROS responses to temperature and precipitation is analyzed using a physically based snow model, forced with reanalysis climate data (1980 – 2019) perturbed according to a range of temperature and precipitation changes consistent with 21st century climate projections ~~spread~~ for the mountain range (Amblar-Francés et al., 2020). Previous studies in alpine zones have shown different ROS response to warming depending on the area and month of the season (e.g., Morán-Tejeda et al. 2016). For this reason, results are focused on these two factors. First, we analyze height of snow (HS) and snowfall fraction (Sf) responses to temperature and precipitation since these are the main variables that control ~~main drivers of~~ ROS events (López-Moreno et al., 2021). Next, we examine ROS patterns and their response to warming by three key ROS indicators, namely:

(a) Number of ROS days for a season (ROS frequency).

(b) Average rainfall quantity during a ROS day (ROS rainfall amount).

(c) Average daily snow ablation during a ROS day (ROS ablation).

The study area is presented in Section 2. Section 3 describes the data and methods. Section 4 presents the results. We finally discuss the anticipated ROS spatio-temporal changes, their socio-environmental impacts and hazards in Section 5.

2 Regional setting

~~The Pyrenees mountain~~The Pyrenees Mountain range is located between the Atlantic Ocean (West) and the Mediterranean Sea (East~~), and~~) and is the largest (~ 450 km) mountain range of the Iberian Peninsula. Elevation increases towards the central massifs, where the highest peak is found (Aneto, 3,404 m asl). Glaciers expanded during the Little Ice Age and nowadays ~~are located in~~are in the highest mountain summits (Vidaller et al., 2021). The regional annual 0 °C isotherm is at ca. 2700 m (Del Barrio et al., 1990), and at ca. 1600 m during the cold season (López-Moreno and Vicente-Serrano, 2011). The elevation lapse-rate is ca. 0.6º/100 m, being slightly lower during winter (Navarro-Serrano and López-Moreno, 2017). Annual precipitation is ca. 1000 mm/year (ca. 1500 m); maximum values are found in the northern-western massifs (around 2000 mm/year), decreasing towards the southern-eastern (SE) area (Lemus-Canovas et al., 2019). Precipitation is predominantly (> 90%) solid above 1600 m from November to May (López-Moreno, 2005). Due to the mountain ~~alignement~~alignment, relief configuration, and the distance to the Atlantic Ocean, seasonal snow accumulations in the northern slopes (ca. 500 cm/season), almost doubles the recorded in the SE area for the same elevation (ca. 2000 m) (Bonsoms et al., 2021b). In the western and central area of the southern slopes of the range (SW sector, Figure 1), snow accumulation is ruled by Atlantic wet and mild flows, which are linked with negative North Atlantic Oscillation (NAO) phases (SW and W synoptic weather types) (López-Moreno, 2005; Alonso-González et al., 2020b; Bonsoms et al., 2021a). Positive Western Mediterranean Oscillation (WeMO) phases (NW and NE synoptic weather types) control the snow patterns in the northern-eastern (NE) slopes of the range (Bonsoms et al., 2021a). Generally, snow ablation starts in February at~~y in~~ low elevations and in May at high elevation. The energy available for snow ablation is controlled by net radiation (55 %, over the total), latent (32 %) and sensible (13 %) heat fluxes (Bonsoms et al., 2022).

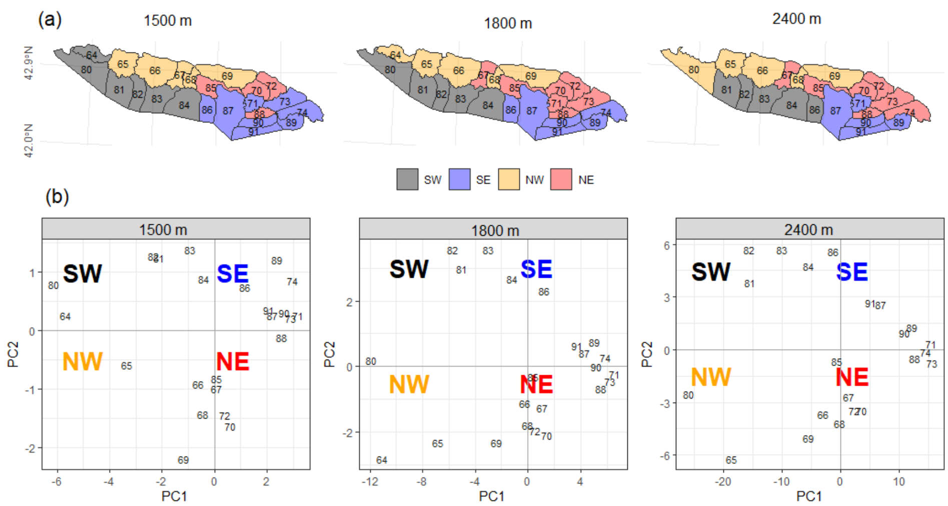

Figure 1. (a) Pyrenean massifs sectors (colors) for 1500 m, 1800 m and 2400 m elevation. Massifs were classified according to a Principal Component Analysis (PCA) applied over monthly HS data of each massif and elevation range for all months and years of the historical climate period (1980 – 2019). (b) ~~Principle~~PCA ~~Component Analysis (PCA)~~ scores of each massif for 1500 m, 1800 m and 2400 m elevation. The black numbers are the SAFRAN massif's identity numbers defined by Vernay et al. (2022). Note that 2400 m~~high~~ elevation does not include massif number 64 since this massif does not reach that elevation range.~~2400 m~~.

3 Data and methods

3.1 Snow model description

Con formato: Inglés (Estados Unidos)

The ~~Sn~~snowpack is ~~modeled~~simulated using the energy and mass balance snow model FSM2 (Essery, 2015). The FSM2 was forced at hourly resolution for each massif and elevation range (c.f. Sect. 3.3) for the ~~baseline climate~~historical climate period (1980 – 2019) and perturbed ~~according to climate projections~~using a range of values of temperature and -precipitation changes consistent with 21st century climate projections (c.f. Sect. 3.4). Sf was quantified using a threshold-approach. Precipitation was snowfall when temperature was < 1 ºC according to previous ROS research in the study zone (Corripio and López-Moreno, 2017) and the average rain-snow temperature threshold for the Pyrenees (Jennings et al., 2018). Snow cover fraction is calculated by a linear function of snow depth, snow albedo is estimated based on a prognostic function with the new snowfall. Snow thermal conductivity is estimated based on snow density. Liquid water percolation is calculated based on a gravitational drainage. Compaction rate is simulated from overburden and thermal metamorphism. The atmospheric stability is estimated through the Richardson number stability functions to simulate latent and sensible heat fluxes. The selected FSM2 configuration includes three snow layers and four soil layers. The ~~detailed~~ FSM2 ~~physical parameters~~configuration selected ~~and Fortran compilation numbers are~~ is shown in Table S1. The FSM2 model and configuration was previously validated in the Pyrenees at Bonsoms et al. (2023). FSM2 has been successfully used in snow model sensitivity studies in alpine zones (Günther et al., 2019). FSM2 has been implemented in a wide range of alpine conditions, such as for the Iberian Peninsula mountains (Alonso-González et al., 2019), Spanish Sierra Nevada (Collados-Lara et al., 2020) or ~~swiss~~Swiss forest environments (Mazzotti et al., 2020) snowpack modeling. FMS2 has been integrated in snow data-assimilation schemes in combination with in-situ (Smyth et al., 2022) and remote-sensing data (Alonso-González et al., 2022).

3.2 Atmospheric forcing data

The FSM2 was forced with the SAFRAN meteorological system reanalysis dataset for flat terrain (Vernay et al., 2022). The SAFRAN meteorological system integrates meteorological simulations, remote-sensing cloud cover data, and instrumental records through data-assimilation. SAFRAN is forced with a combination of ERA-40 reanalysis (1958 to 2002) and the numerical weather prediction model ARPEGE (2002 to 2020). SAFRAN system was firstly designed for ~~avalanche monitoring~~hazard forecasting (Durand et al., 1999, 2009)~~, but the accurate results obtained enhanced the diffusion of the meteorological system and its integration in the French hydrometeorological modelling system by the local weather service, Metéo France (Habets et al., 2008).~~ SAFRAN has been extensively validated as meteorological forcing data for the snow modeling in complex alpine terrain (Revuelto et al., 2018; Deschamps-Berger et al., 2022), to study long-term snow evolution (Réveillet et al., 2022), avalanche hazard forecasting (Morin et al., 2020), snow climate projections (Verfaillie et al., 2018), snow depth (López-Moreno et al., 2020) and energy heat fluxes spatio-temporal trends (Bonsoms et al., 2022).

3.3 Spatial areas

SAFRAN system provides data at hourly resolution from 0 to 3600 m, by steps of 300 m, grouped by massifs. The SAFRAN massifs (polygons of Figure 1) were chosen for their relative topographical and climatological similarities (Durand et al., 1999). We selected the 1500 m (low), 1800 m (mid), and 2400 m (high) specific elevation bands of the Pyrenees. In order to retain the main spatial differences across the mountain range, reduce data dimensionality and include the maximum variance, massifs with similar interannual snow characteristics were grouped into sectors by performing a Principal Component Analysis (PCA). PCA is an extensively applied statistical method for climatological and snow spatial regionalization (i.e., López-Moreno and Vicente-Serrano, 2007; Schöner et al., 2019; Alonso-González et al., 2020a; Matiu et al., 2021; Bonsoms et al., 2022). A PCA was applied over HS data for all months and years of the ~~baseline climate~~historical climate period. Massifs were grouped into four groups depending on the maximum correlation to the first (PC1) and second (PC2) scores. Pyrenean sectors were named South-West (SW), South-East (SE), North-West (NW) and North-East (NE) due to their geographical position. Figure 1 shows the resulting Pyrenean regionalization for 1500 m, 1800 m and 2400 m~~high~~ elevation as well as the SAFRAN massifs PC1 and PC2.

3.4 Sensitivity analysis

ROS season extension was defined according to ROS occurrence during the ~~baseline climate period~~historical climate period. For the purposes of this research, seasons are classified as follows: October and November (Autumn); December, January, and February (Winter); March, April, May, and June (Spring); and July (Summer). August and September are not included due to the absence of regular snow cover. ~~ROS sensitivity to precipitation, Ta, increasing incoming longwave radiation (Lwin)~~ Sf, HS and ROS sensitivity to air temperature and precipitation ~~accordingly~~is analyzed by perturbing climate data (López-Moreno et al., 2013; Pomeroy et al., 2015; Marty et al., 2017; Musselman et al., 2017b; Rasouli et al., 2019; Alonso-González et al., 2020a; López-Moreno et al., 2021).~~. This method has been successfully applied and validated for analyzing the snow sensitivity to temperature and precipitation changes in many mountains, such as the Pyrenees (e.g., López-Moreno et al., 2013), the Iberian Peninsula mountain areas outside the Pyrenees (Alonso-González et al., 2020a), Alps (Marty et al., 2017), Canadian basins (Pomeroy et al., 2015; Rasouli et al., 2019), or western United States (Musselman et al., 2017b), among other works. This methodology has also been also performed in global ROS sensitivity to temperature change studies (López-Moreno et al., 2021).~~ Specifically, SAFRAN reanalysis climate data was perturbed according to Spanish Meteorological Agency ~~climate change scenarios projected~~ air temperature and precipitation projections for the 21st ~~c~~Century in the Pyrenees (Amblar-Francés et al., 2020). Precipitation was increased (+10%), left unchanged (0 %) and decreased (- 10%). Air temperature~~Ta~~ (ºC) was perturbed ~~from~~ between +1ºC and~~to~~ +4ºC by steps of +1ºC. Incoming longwave radiation ~~Lwin~~ was increased due to warming, by applying the Stefan-Boltzmann law, using the Stefan-~~Botzmann~~Boltzmann constant (σ; 5.670373 x $10^{-8} W\ m^{-2}\ K^{-4}$), and the hourly atmospheric emissivity (ϵ_t) derived from SAFRAN ~~Ta and Lwin:~~air temperature and incoming longwave radiation:

$$\epsilon_t = \frac{LW_{in}}{\sigma(Ta + 273.15)^4}$$

Where Ta is air temperature and LWin is incoming longwave radiation. An increase of air temperature ~~temperature increase~~ of 1ºC can be interpreted as a~~n~~ ~~optimistic~~ low ~~projection~~ emission scenario for the region, while 2ºC and 4ºC would represent projections for mid and high emission scenarios, respectively (Pons et al., 2015). The range of +/-10% for precipitation includes the expected changes in precipitation according to ~~the vast majority of~~most climate models, regardless of the emission scenario (López-Moreno et al., 2008; Pons et al., 2015; Amblar-Francés et al., 2020).

3.5 ROS definition and indicators

The average HS and Sf sensitivity to temperature and precipitation (expressed in % per ºC of local warming) is the average seasonal HS and Sf anomalies under the ~~baseline climate~~historical climate period and divided by degree of warming. Days are classified as ROS days when daily rainfall amount was >= 10 mm and HS >= 0.1 m, according to previous works (Musselman et al., 2018; López-Moreno et al., 2021). ROS frequency ~~are~~is the number of ROS days. ROS rainfall amount (mm/day) is the average daily rainfall (mm) during a ROS day. ROS ablation is the average daily snow ablation (cm/day) during a ROS day. The average daily snow ablation is the daily average HS difference between two consecutive days (Musselman et al., 2017a). Only the days when a negative HS difference ~~ocured~~occurred were selected. ~~ROS exposure is the relation between ROS rainfall amount (y axis) and ROS frequency (x axis) differences from the baseline climate scenario for the massifs were ROS frequency is recorded for all increments of temeperature.~~

4 Results

We provide an analysis of ~~ROS drivers~~Sf, HS, ~~near-present~~and ROS patterns ~~and their~~ response to ~~-~~ temperature and precipitation change~~warming~~. ROS spatio-temporal dynamics are analyzed in terms of~~by~~ frequency, rainfall quantity and snow ablation. Since we have detected a non-linear ~~and counter-intuitive~~ ROS sensitvity to temperature, ROS indicators values are shown ~~for each increment of temperature~~as a function of the change in temperature and precipitation amounts, grouped by elevation and sectors, namely SW, SE, NW and NE.

4.1 HS and Sf response to temperature and precipitation change

HS and Sf response to temperature and precipitation is shown in Figure 2. Seasonal HS and Sf variability is mostly controlled by the increment of temperature, season, elevation, and spatial sector. The role of precipitation variability in the seasonal HS evolution is moderate to low~~1500 m~~ (Figure S1 to S3). Only at~~in~~ 2400 m elevation an upward trend of precipitation (at least > 10%) can counterbalance small increments of temperature (< 1ºC, over the ~~baseline climate~~historical climate period) from December to February (Figure

S4~~3~~). For this reason, precipitation was excluded to further analysis, and the ROS sensitivity analysis is evaluated for the average change of precipitation. Snow at~~in~~ 1500 m and 1800 m elevations during summer is rarely observed, however, marginal snow cover at~~in~~ 2400 m elevation can last until June and July, especially in the wettest sectors of the range (NW and SW). Seasonal HS and Sf response to temperature show large seasonality. The average HS ~~decrease~~reduction ~~per ºC~~ ranges from 39 %, 37 % and 28 % per ºC, for 1500 m, 1800 m and 2400 m elevations, respectively. However, relevant differences are found depending on the season and degree of warming (Figure 3). Maximum HS and Sf reductions are found in 1500 m and 1800 m elevations during the shoulders of the season (autumn and spring). ~~, coinciding with the time when ROS events are more frequent for the baseline climate (Figure 3).~~ In these elevations, maximum HS decreases (52 % over the ~~baseline climate~~historical climate period) are ~~modeled~~simulated for spring when temperature is + 1ºC. The greatest HS decreases in 2400 m elevation areas are ~~modeled~~simulated for summer (54 % HS decrease for 1ºC). If temperature reaches maximum values (+ 4 ºC), seasonal HS is reduced by 92 %, 89 %, and 79 % for 1500 m~~low~~, 1800 m, and 2400 m elevations, respectively (Figure S4).

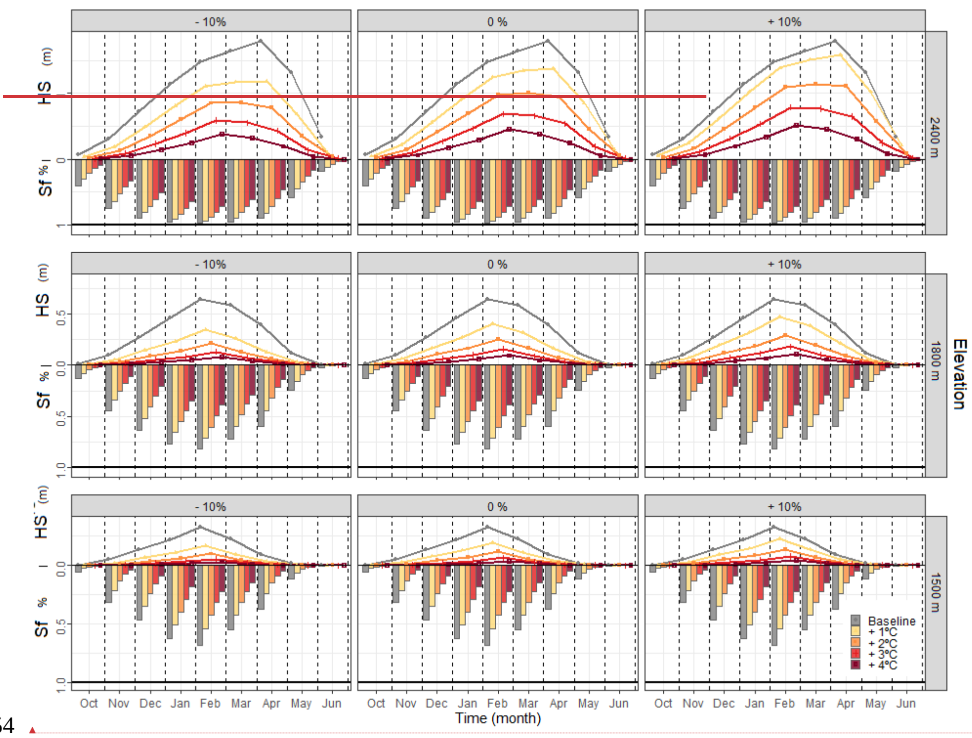

Con formato: Inglés (Estados Unidos)

Con formato: Inglés (Estados Unidos)

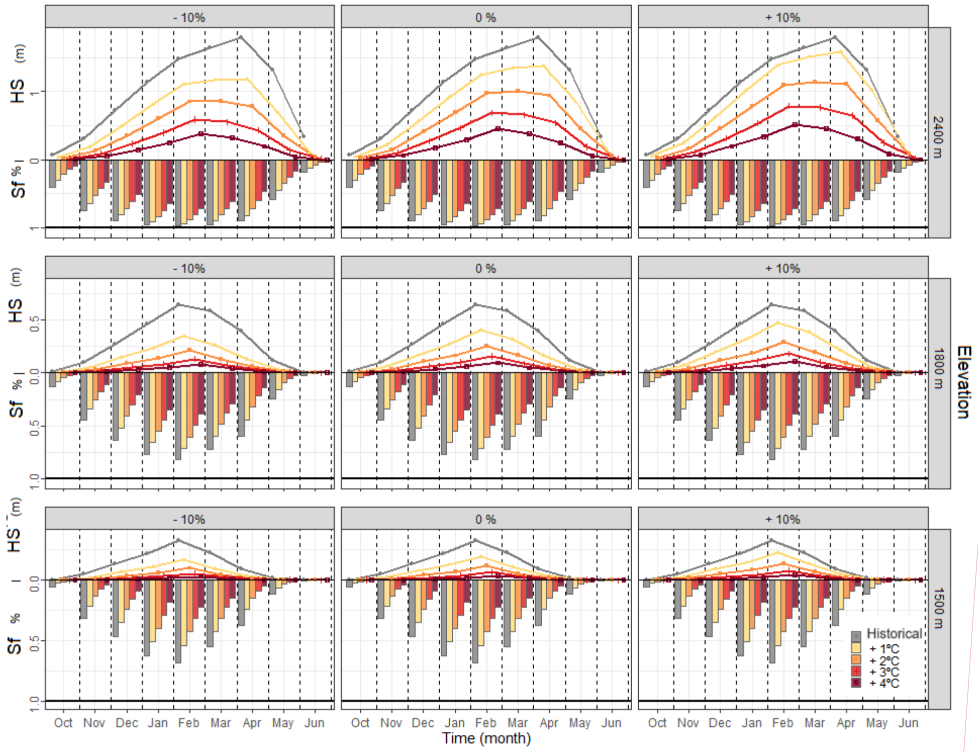

Figure 2. Height of snow (HS) (lines) and Snowfall fraction (Sf) (bars) monthly variation for the ~~baseline climate~~historical climate period (1980 – 2019) ~~scenario~~ and different increments of temperature (colors) grouped by precipitation change and elevation (~~rows~~boxes). Note that Sf values (y-axis) are inverted. ~~and sectors (columns).~~

Con formato: Inglés (Estados Unidos)

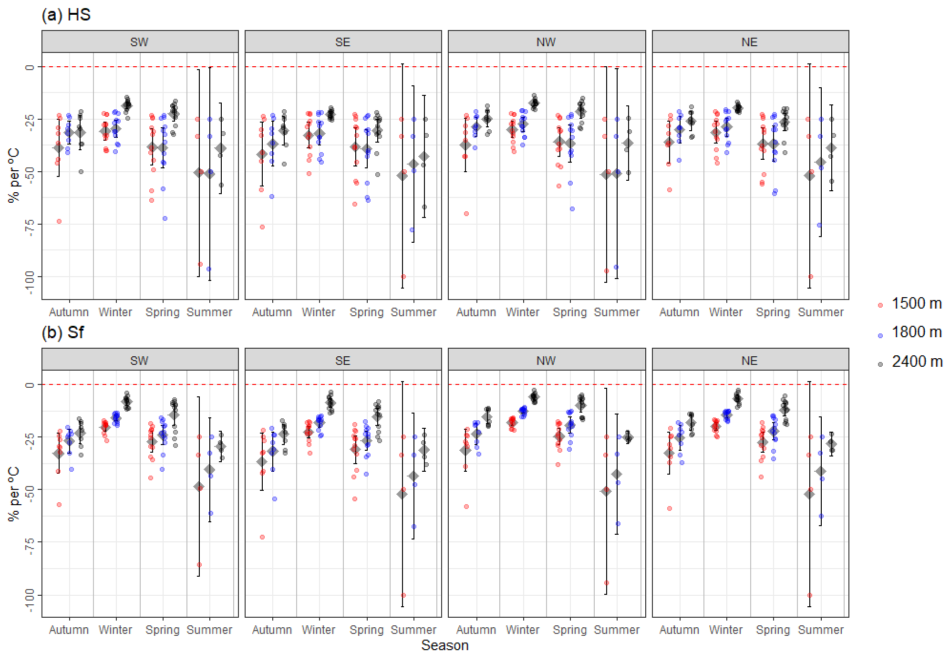

Figure 3. Seasonal (a) HS and (b) Sf anomalies over the ~~baseline climate~~historical climate period (1980 – 2019). ~~.~~Data are shown by elevation (colors), season (x-axis) and sectors (boxes). Points represent the average seasonal HS and Sf anomalies grouped by month of the season and increment of temperature (from 1ºC to 4ºC). The black diamond point indicates the mean, whereas the upper and lower error bars show the Gaussian confidence based on the normal distribution. Data are the average of the simulated precipitation change (from -10% to 10%, by steps of 10%).

Sf shows lower sensitivity to warming than HS and maximum reductions in autumn. On average, Sf decreases by 29%, 22 %, and 12 % per ºC for 1500 m~~low~~, 1800 m, and 2400 m elevations, respectively. An increase of 4ºC ~~supposes~~ leads to Sf reductions of 80 %, 69 % and 49 % for 1500 m~~low~~, 1800 m, and 2400 m elevations. ~~Different HS and Sf sensitivity to temperature are found across the range.~~ Independently of the elevation band and season, the SE sector exhibit the greatest HS and Sf decreases (41 % and 35 % per ºC, respectively). On the contrary, minimum reductions are expected in the northern slopes (NW and NE).

4.2 ROS frequency

During the historical climate period (1980 – 2019), annual ROS frequency totals on average 10, 12 and 10 day/season for 1500 m, 1800 m and 2400 m elevations. However, there are large differences depending on the sector. 1500 m~~Low~~ elevation annual ROS frequency for the ~~baseline climate~~historical climate period -is 17, 8,

Con formato: Inglés (Estados Unidos)

Con formato: Inglés (Estados Unidos)

Con formato: Inglés (Estados Unidos)

10 and 7 days/year for SW, SE, NW, NE sectors, respectively (Figure 4). The highest annual ROS frequency is however observed at 1800 m elevation. Here, annual ROS frequency is 17, 9, 12 and 9 for SW, SE, NW, NE sectors. Within these elevations, the maximum ROS frequency is detected in SW during winter and spring (7 days/season, for both elevations and seasons). The eastern Pyrenees follow a similar seasonality. Maximum ROS frequency at~~in~~ 1500 m elevation is found in winter (4 and 3 days/season, SE and NE, respectively), and during spring at~~in~~ 1800 m elevation (4 and 3 days, SE and NE, respectively). ROS is rarely observed in SE during the latest month of spring (May), which contrast with the ~~modeled~~simulated values for SW (2 and 3 days/month, for 1500 m and 1800 m elevations, respectively). 2400 m elevation shows the minimum ROS frequency. Here, comparisons between seasons reveal maximum ROS frequency during summer, especially in SW (7 days/season), followed by NW (6 days/season), and NE (2 days/season).

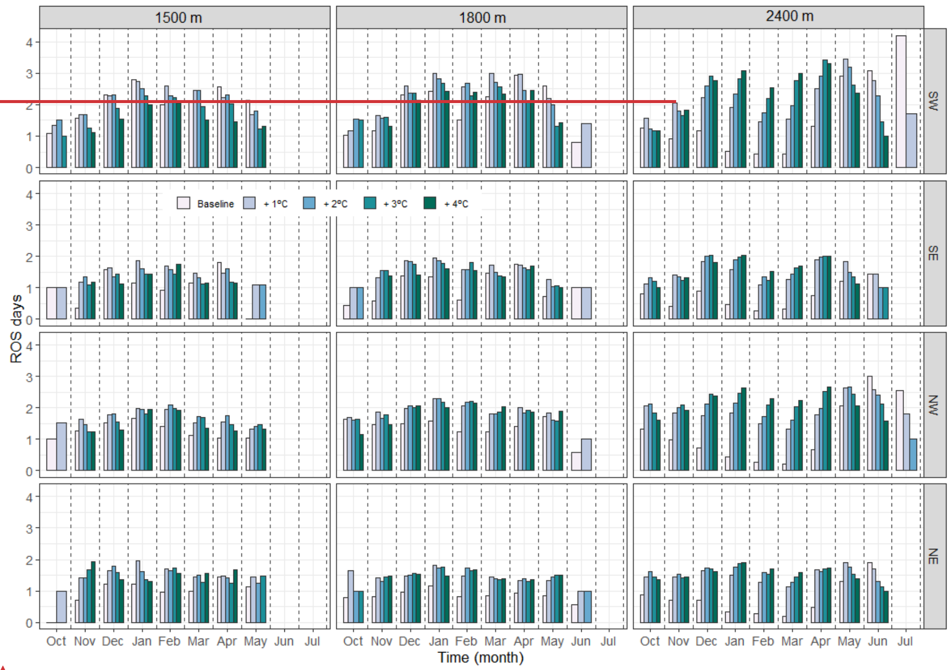

Con formato: Inglés (Estados Unidos)

Con formato: Inglés (Estados Unidos)

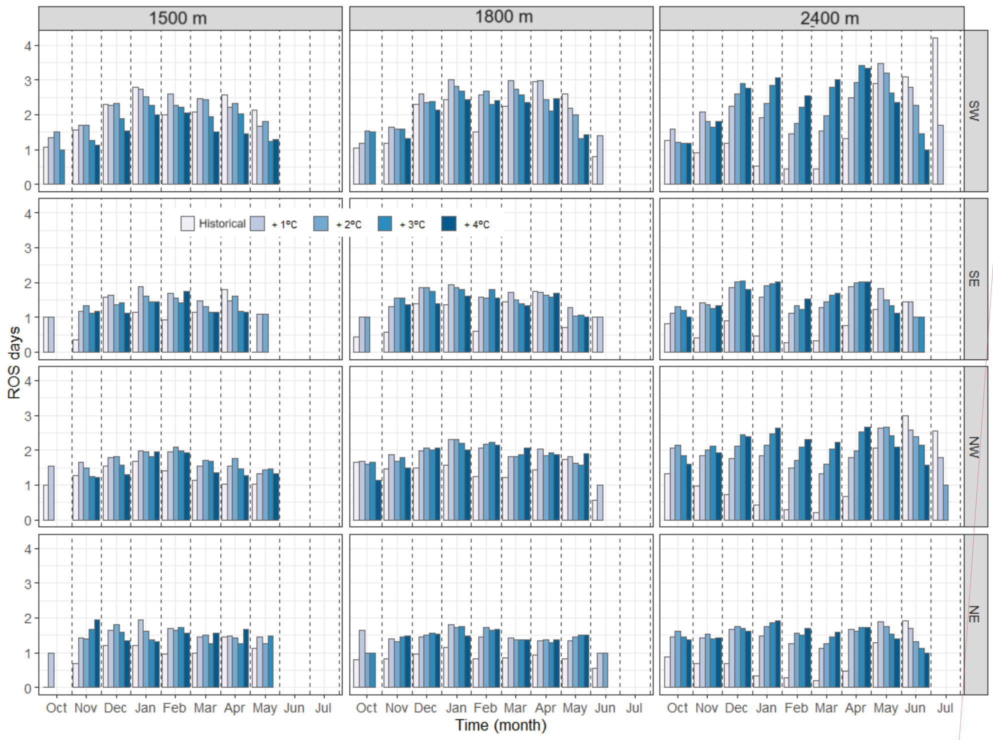

Figure 4. ROS frequency for ~~baseline climate period~~the historical climate period (~~1980-2019~~1980 – 2019) and increments of temperature (colors), grouped by months (x-axis), sector (rows) and elevation (columns). Data are the average of the simulated precipitation change (from -10% to 10%, by steps of 10%).

ROS frequency response to warming vary depending on the month, increment of temperature, elevation, and sector. ROS tends to disappear in October for 1500 m elevation for + 1ºC, except in SW (Figure 4 and 5). The highest increases are seen during the winter for increments temperature lower than 3ºC, particularly in NE, where ROS frequency increases 1 day per month over the ~~baseline scenario~~historical climate period for + 1ºC. At~~In~~ 1800 m elevation, ROS frequency increases in all regions from November to February (around 1 day per month, for + 1ºC up to + 3ºC). Similar increases are expected in NW and SW during the earliest months of spring and for 1500 m to moderate increments of temperature. The contrary is observed during the latest months of spring in SW, where warming reduces ROS events. A slight ROS frequency increase is found during spring for the rest of the sectors (Figure 4). ROS events in June are expected to disappear for temperature increases higher than 1ºC. Finally, 2400 m elevation shows the largest ROS frequency variations (around 1 day/month for + 1ºC). Maximum ROS frequency increases (3 days/month) are found in SW for more than + 3ºC. ROS frequency progressively increases in March and April for all sectors but tends to decrease in May (for + 3ºC), June and July (for + 1ºC).

Con formato: Inglés (Estados Unidos)

Con formato: Centrado

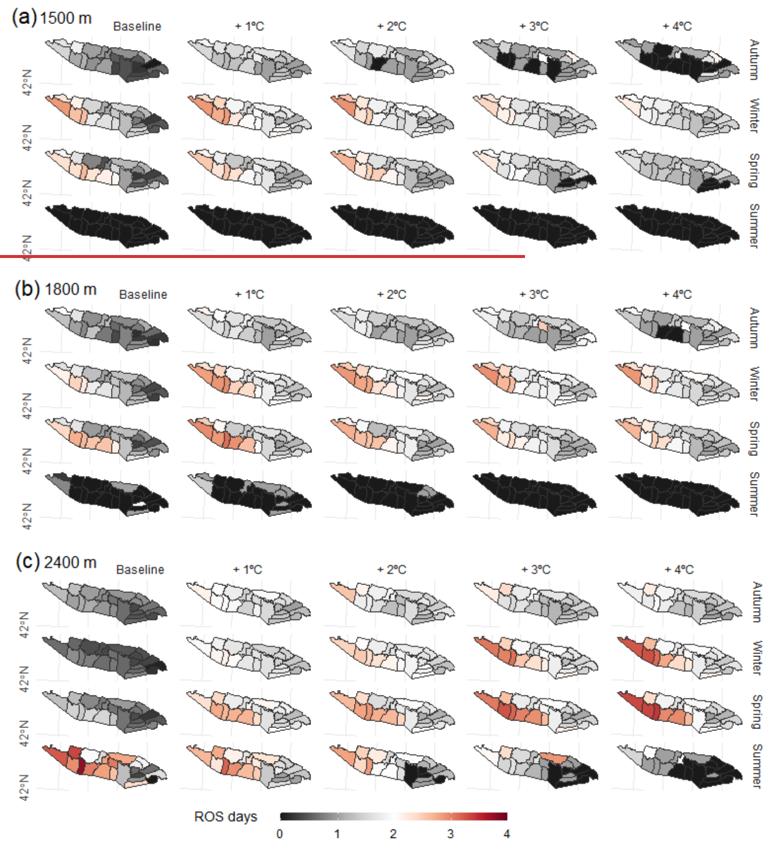

Con formato: Centrado

Con formato: Inglés (Estados Unidos)

Con formato: Inglés (Estados Unidos)

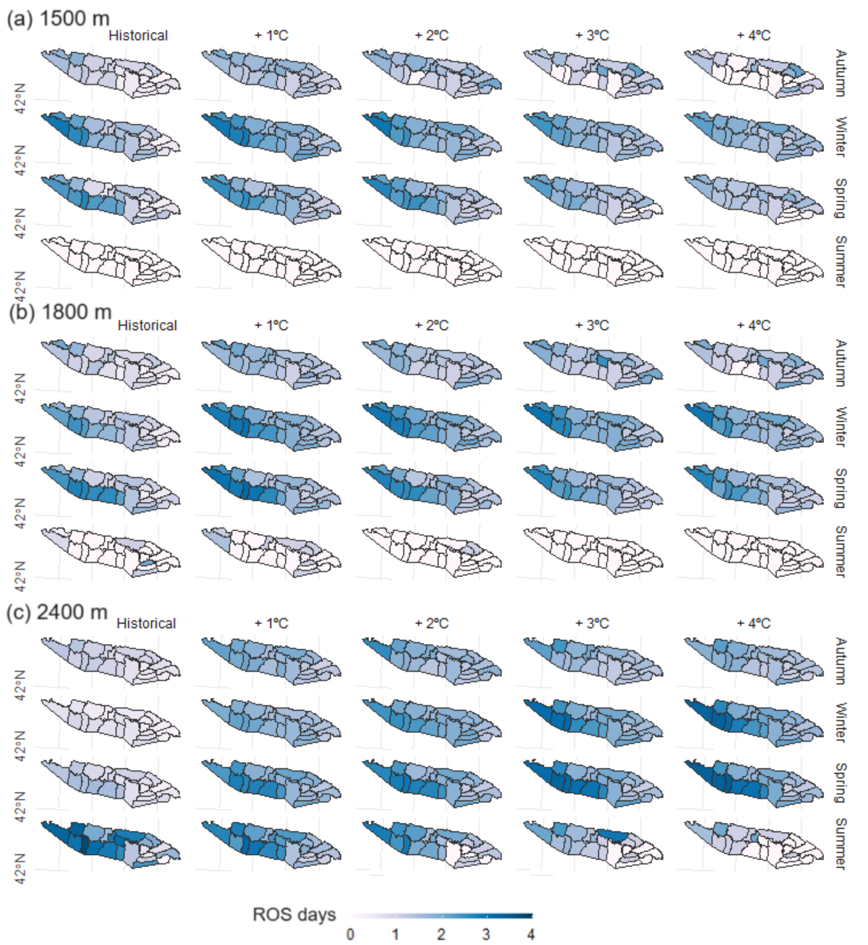

Figure 5. Average ROS frequency (days) for a season for (a) 1500 m, (b) 1800 m and (c) 2400 m elevation. Data are shown for the ~~baseline climate period~~historical climate period, (~~1980-2019~~1980 – 2019,) and increment of temperature (left to right). Data are the average of the simulated precipitation change (from -10% to 10%, by steps of 10%).

4.3 ROS rainfall amount

The spatial and temporal distribution of ROS rainfall amount is presented in Figure 6 and 7. The average 1500 m elevation ROS rainfall amount by year is 23, 28, 21, and 20 mm/day for SW, SE, NW, NE sectors, respectively. ~~Similarly, the highest values~~ At~~in~~ 1800 m elevation, the highest ROS rainfall amount values are also found in SE (29 mm/day~~, respectively~~). Particularly, SE sector experiences the highest ROS rainfall amount during autumn and summer (around 40 mm/day at~~in~~ 1500 m and 1800 m elevations). At 2400 m

Con formato: Inglés (Estados Unidos)

Con formato: Inglés (Estados Unidos)

Con formato: Inglés (Estados Unidos)

Con formato: Fuente: 12 pto

elevation, however, ~~-~~maximum ROS rainfall amount values ~~are however~~ are found in ~~the western~~SW and NW ~~Pyrenees~~ during ~~the onset and offset snow season~~autumn. Here, the largest ROS rainfall amount spatial and seasonal distribution ranges from SW (29 mm/day, autumn), NW (28 mm/day, summer), SE (24 mm/day, autumn) to NE (23 mm/day, autumn).

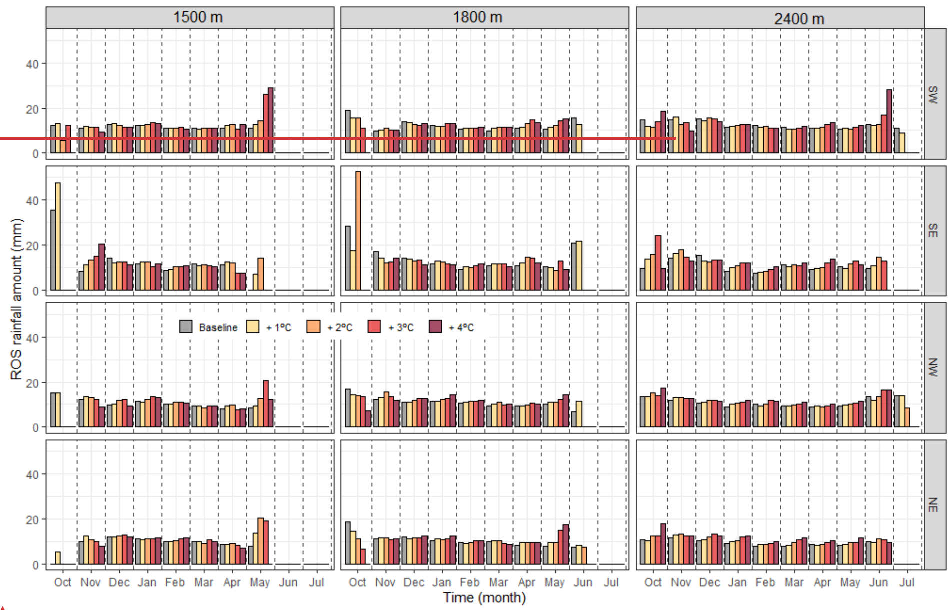

Con formato: Inglés (Estados Unidos)

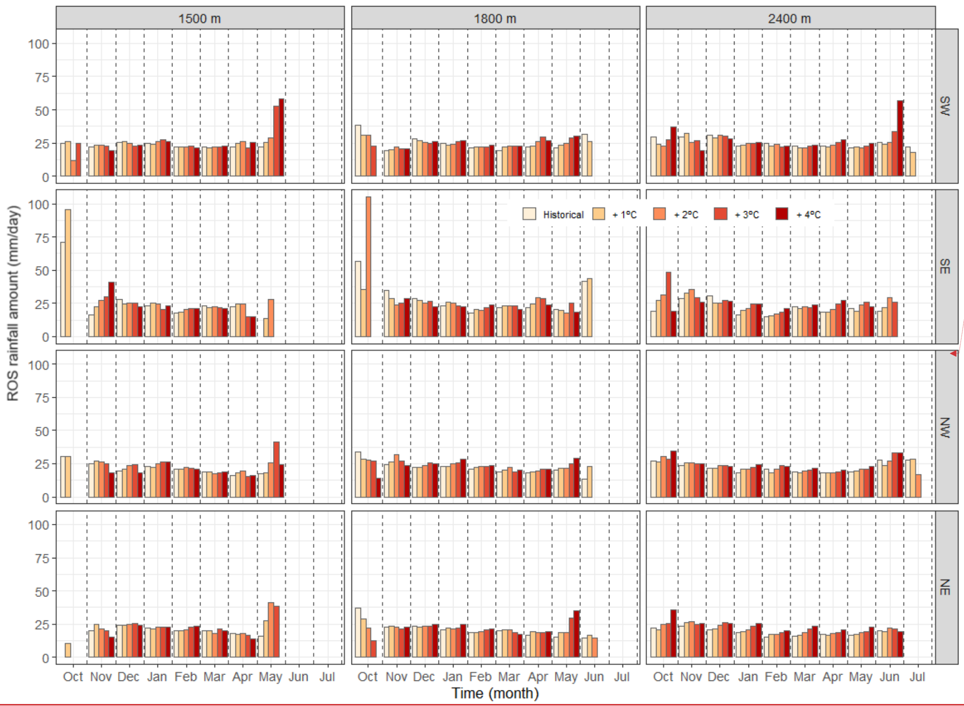

Figure 6. Average ROS rainfall amount (mm/day) for each month of the season. Data are shown for the historical climate period (1980 – 2019) and different increments of temperature (colors), grouped by month (x-axis), elevation and sector (boxes). Data are the average of the simulated precipitation change (from -10% to 10%, by steps of 10%).

~~**Figure 6.** ROS rainfall amount (mm) temporal evolution for baseline climate (1980-2019) and increment of warming (colors), grouped by elevation (columns) and sector (rows).~~

ROS rainfall amount ~~progressevly~~progressively increases due to warming (4%, 4%, and 5% per ºC for 1500 m~~low~~, 1800 m, and 2400 m elevations, respectively; Table S2). Small differences are found by elevation and sector. 1500 m elevation ROS rainfall amount increases until + 3°C, and generally decreases for + 4°C during the earliest (October to December) and latest (April and May) months of the snow season. Similar patterns are found at~~in~~ 1800 m elevation. ROS rainfall amount increases up to + 4°C, except in the SE sector for specific months (Figure 6). The ~~lattest~~latest sector shows also maximum ROS rainfall amount values in autumn due to torrential rainfall. 2400 m elevation ROS rainfall amount increase at a constant rate of around 5 % per ºC. Yet, maximum increases are ~~modeled~~simulated in SW during summer, when ROS rainfall amount almost doubles the ~~baseline climate~~historical climate period (+ 40% for + 4°C).

Con formato: Centrado

Con formato: Izquierda

Con formato: Inglés (Estados Unidos)

Con formato: Inglés (Estados Unidos)

Con formato: Inglés (Estados Unidos)

Con formato: Inglés (Estados Unidos)

Con formato: Inglés (Estados Unidos)

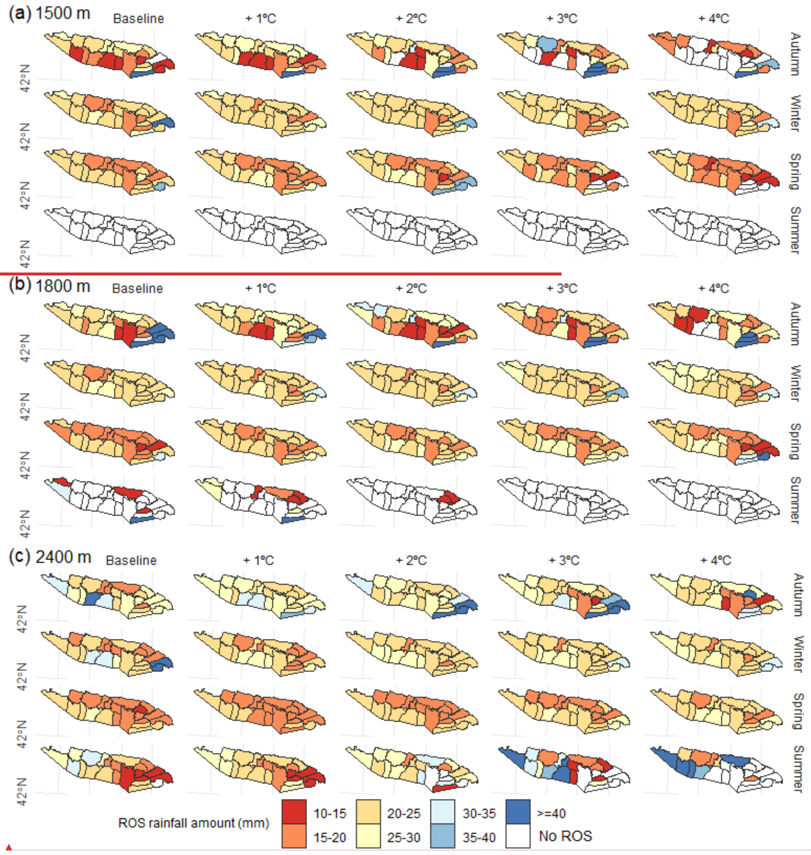

Con formato: Inglés (Estados Unidos)

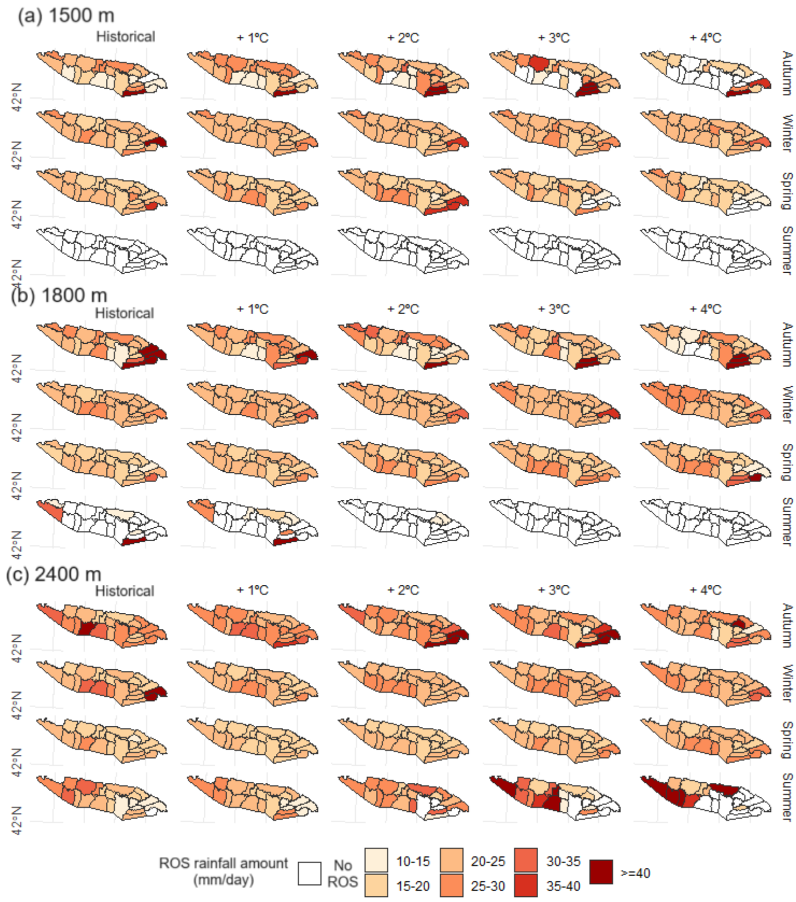

Figure 7. Average ROS rainfall amount (mm/day) for a season (rows) for (a) 1500 m, (b) 1800 m and (c) 2400 m elevation. Data are shown for the ~~baseline climate period~~historical climate period (~~1980-2019~~1980 – 2019) and increment of temperature (columns)~~left to right~~). Data are the average of the simulated precipitation change (from -10% to 10%, by steps of 10%).

Data suggest that ROS ~~exposure~~ rainfall amount and frequency generally increases for all elevations and sectors during winter (except in SW for temperatures greater than 3°C) (Figure 8). Nonetheless, ~~remarckable~~remarkable spatial and seasonal differences are found. SE shows the maximum values in autumn. On the contrary, small changes in frequency are detected in SW and NW, despite ROS rainfall amount is expected to increase (< 10 mm/day). For ~~the majority of~~most sectors and elevations, ROS ~~exposure~~ rainfall amount and frequency generally increases in winter and spring. The minimum differences between sectors are ~~dected~~detected in these seasons. In summer, ROS ~~exposure~~ rainfall amount and frequency tends to generally decrease for all elevations under severe warming due to snow cover depletion.

Con formato: Inglés (Estados Unidos)
Con formato: Inglés (Estados Unidos)
Con formato: Inglés (Estados Unidos)
Con formato: Inglés (Estados Unidos)
Con formato: Inglés (Estados Unidos)
Con formato: Inglés (Estados Unidos)
Con formato: Inglés (Estados Unidos)
Con formato: Inglés (Estados Unidos)
Con formato: Inglés (Estados Unidos)
Con formato: Inglés (Estados Unidos)
Con formato: Inglés (Estados Unidos)
Con formato: Inglés (Estados Unidos)
Con formato: Inglés (Estados Unidos)
Con formato: Inglés (Estados Unidos)
Con formato: Inglés (Estados Unidos)

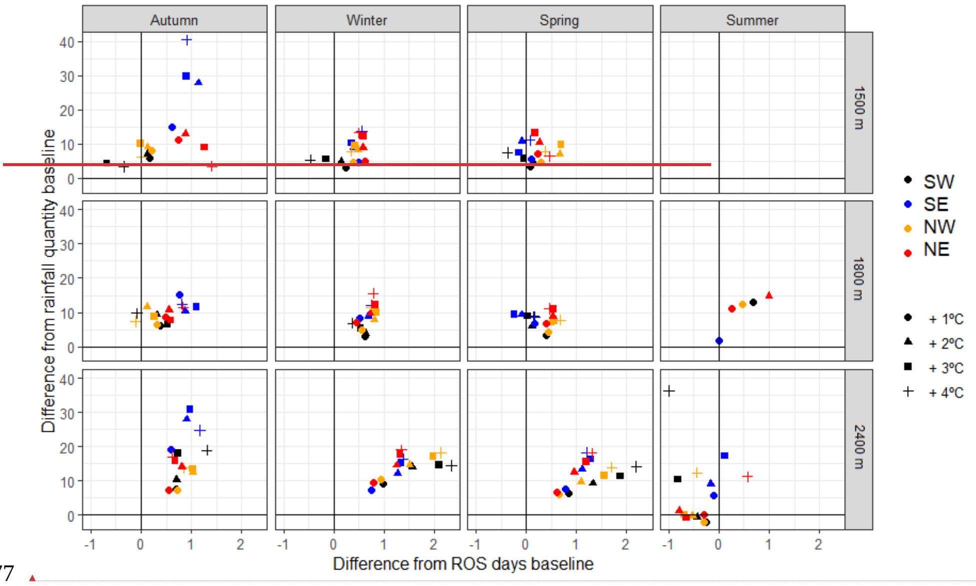

Con formato: Inglés (Estados Unidos)

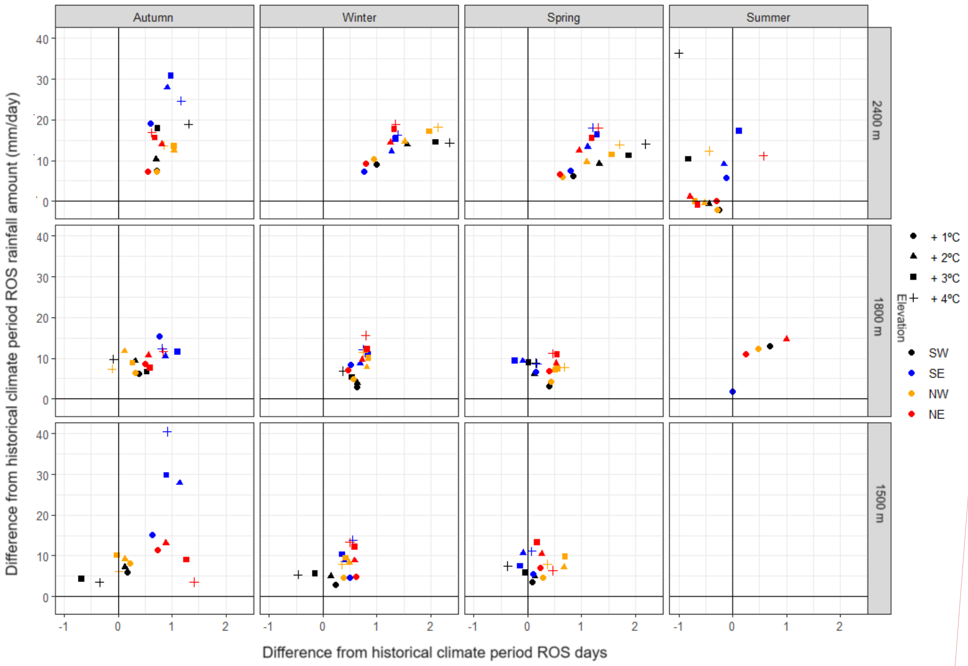

Con formato: Inglés (Estados Unidos)

Figure 8. ~~Average ROS exposure. Points are obtained by a S~~scatterplot between ROS rainfall amount

(mm/day) difference from ~~baseline climate period~~the historical climate period (~~1980-2019~~1980 – 2019) (y-axis) and ROS days difference from ~~baseline climate~~the historical climate period (x-axis). Data is calculated by the average difference between (a) the ~~baseline scenario~~historical climate period values ~~(1980-2019)~~ and (b) the values resulting from the different increments of temperature ~~different perturbed scenarios~~, only for the massifs where ROS frequency exists on (a) and (b). Data are shown for each season (columns), elevation (rows), sector (color) and increment of temperature (point shape). Data are the average of the simulated precipitation change (from -10% to 10%, by steps of 10%).

4.4. ROS ablation

ROS ablation is presented at Figure 9 and 10. ROS ablation ranges from -10 cm/day in NW 2400 m elevation (summer) to – 5 cm/day in NE 2400 m elevation (winter). ROS ablation nearly doubles the average daily snow ablation for all days on a season (Figure S5). Comparison with the reference baseline period reveals contrasting ROS ablation changes depending on the season, elevation and sector. Overall ROS ablation progressively increases due to warming in coldest zones and months of the season. The largest ROS ablation increments are detected in autumn and winter. For the former, ROS ablation increases at a generally constant rate in SW (11 %) NE (19 %) and NW (4 % per ºC). For the latter, ROS ablation increases also in SW (11 %), NW (14 %) and NE (34 % per ºC). In detail, maximum ROS ablation due to warming is found for 1800 m elevation during autumn (Figure 9). ROS ablation exhibit slow and no-changes in the warmest zone (SE), as well in the warmest months of the season, regardless the elevation band.

Con formato: Inglés (Estados Unidos)

Con formato: Inglés (Estados Unidos)

Con formato: Inglés (Estados Unidos)

Con formato: Inglés (Estados Unidos)

Con formato: Inglés (Estados Unidos)

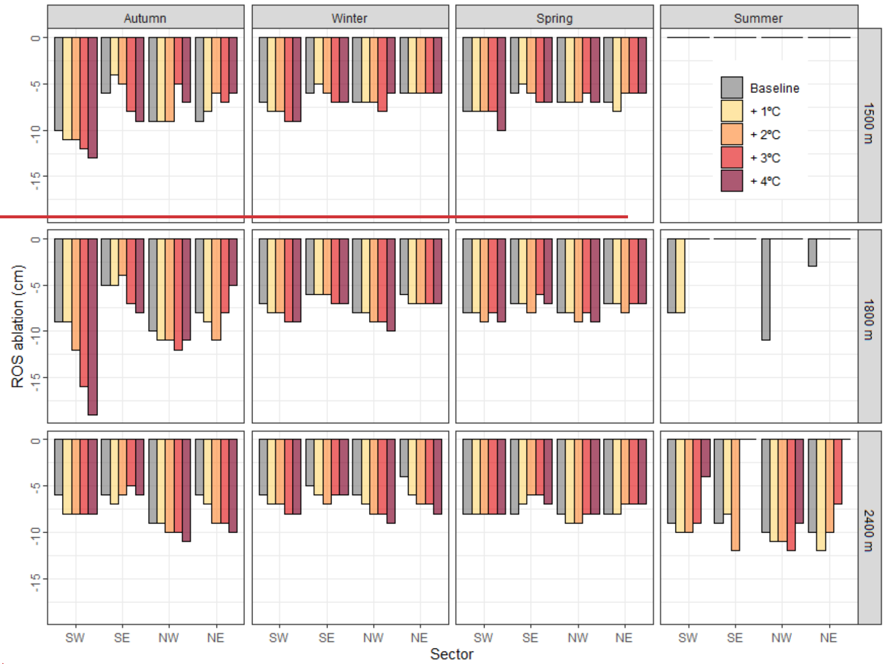

Con formato: Inglés (Estados Unidos)

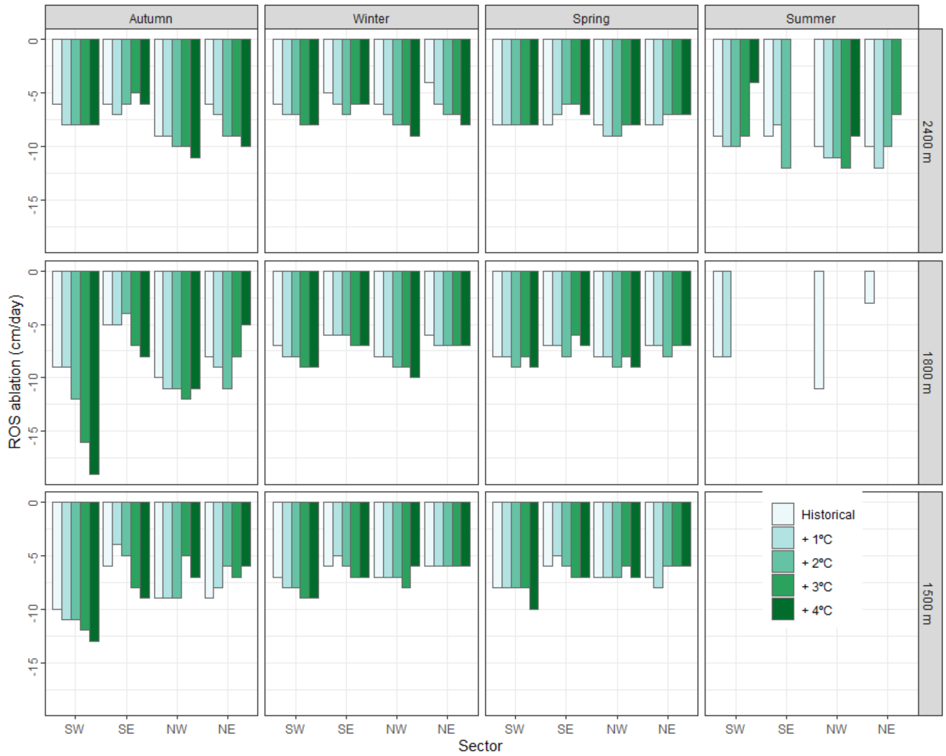

Figure 9. ROS ablation (cm/day; (y-axis) for ~~baseline climate~~the ~~period~~historical climate period (~~1980-2019~~1980 – 2019) and increment of temperature (colors), sector (x-axis), season (columns) and elevation (rows). Data are the average of the simulated precipitation change (from -10% to 10%, by steps of 10%).

Con formato: Inglés (Estados Unidos)

Con formato: Inglés (Estados Unidos)

Con formato: Inglés (Estados Unidos)

Con formato: Inglés (Estados Unidos)

Con formato: Inglés (Estados Unidos)

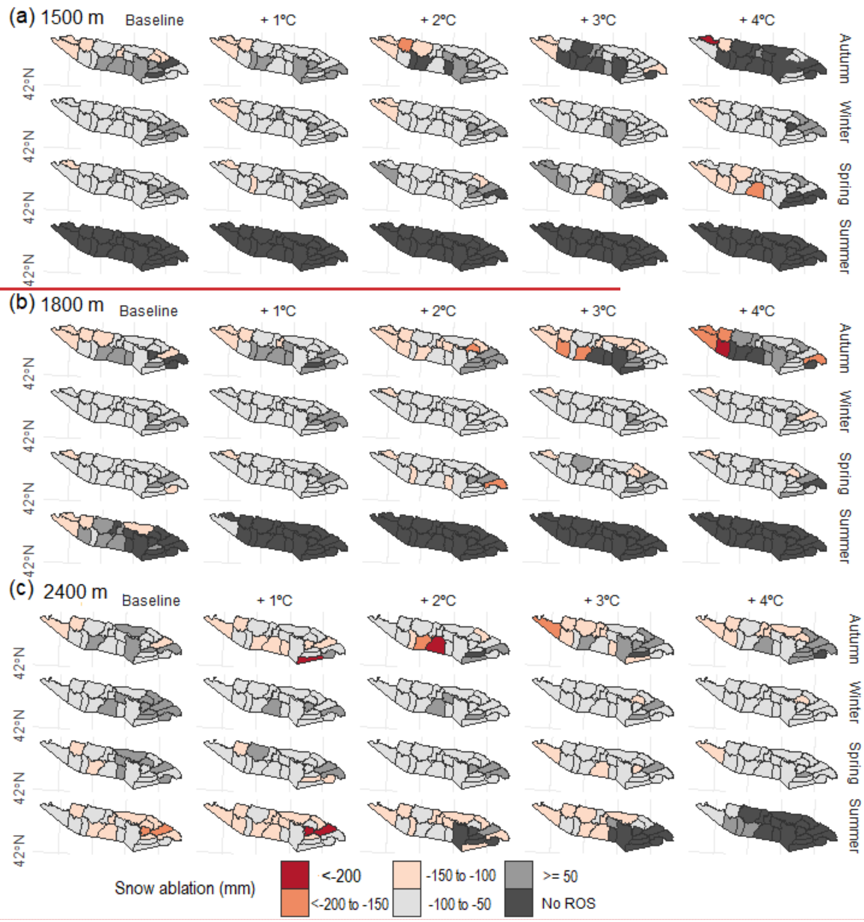

Con formato: Inglés (Estados Unidos)

Con formato: Inglés (Estados Unidos)

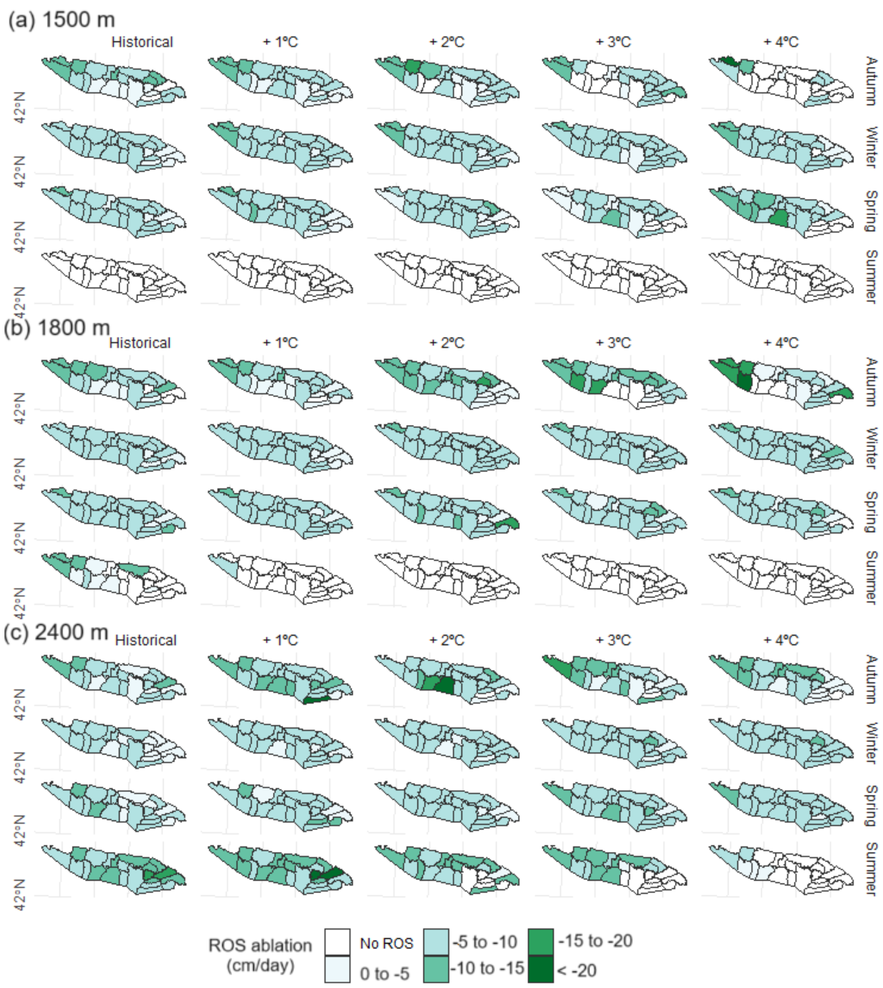

Figure 10. Average ROS ablation (cm/day)~~for a season~~ for (a) 1500 m, (b) 1800 m and (c) 2400 m elevation. Data are shown for the ~~baseline climate period~~historical climate period (~~1980-2019~~1980 – 2019) and increment of temperature (~~left to right).~~columns). Data are the average of the simulated precipitation change (from -10% to 10%, by steps of 10%).

5 Discussion

The Pyrenees experienced a statistically significant positive temperature trend since the 1980s (ca. + 0.2 ºC/decade) but no statistically significant precipitation trends are detected (OPCC, 2018) due to strong spatial

Con formato: Inglés (Estados Unidos)
Con formato: Centrado
Con formato: Inglés (Estados Unidos)
Con formato: Inglés (Estados Unidos)
Con formato: Fuente: 11 pto
Con formato: Inglés (Estados Unidos)
Con formato: Inglés (Estados Unidos)
Con formato: Inglés (Estados Unidos)

(Vicente-Serrano et al., 2017), inter-annual and long-term variability of the latter (Peña-Angulo et al., 2021). Depending on the study period different snow trends were found. From ca. 1980 to 2010, non-statistically significant snow days and snow accumulation positive trends were generally detected at > 1000 m (Buisan et al., 2016), 1800 m (Serrano-Notivoli et al., 2018), and > 2000 m (Bonsoms et al., 2021a). Long-term trends (1957 to 2017), however, reveal ~~statistically significant~~statistically significant snow depth decreases at 2100 m, but large variability depending on the sector and the snow indicator (López-Moreno et al., 2020). Climate projections for the end of the 21st century suggest an increase of temperature (> 3ºC), together with 1500 m precipitation shifts (< 10%) from autumn to spring (Amblar-Francés et al., 2020). Within this climate context, ROS spatio-temporal patterns will likely change. In order to anticipate future ~~scenarios~~ROS patterns, we analyzed ROS sensitivity to warming ~~was analyzed~~ through three key indicators of frequency, rainfall intensity and snow ablation.

Con formato: Inglés (Estados Unidos)

Con formato: Inglés (Estados Unidos)

Con formato: Inglés (Estados Unidos)

5.1 ROS spatial variability

The climatic setting of the Pyrenees as well as its relief configuration determines a remarkable spatial and temporal variability of ROS events. ~~The contradiction between rainfall ratio increases and snowpack reductions, as well as the 2400 m spatial and monthly differences found, explain the complex ROS response to warming.~~ HS decrease by 39 %, 37 % and 28 % per ºC, for 1500 m, 1800 m and 2400 m elevations, respectively. Similarly, Sf decreases by 29 %, 22 %, and 12 % per ºC for 1500 m, 1800 m, and 2400 m elevations. These results provide evidence of an elevation-dependent snow sensitivity to temperature change and are consistent with snow sensitivity to climate works in near alpine sectors, such as the Alps (e.g., Martin et al., 1994). ~~, respectively, providing evidence of an elevation-dependent snow sensitivity to temperature change.~~ HS and Sf maximum reductions are reached for 1ºC of warming, suggesting non-linear HS decreases, in accordance with previous snow sensitivity to climate change reported in central Pyrenees (López-Moreno et al., 2013). The generally ROS rainfall amount increase reported in this work, independently of the increment of temperature and elevation, is explained by the Sf reduction expected for all sectors (Figure 3). Large increments of warming decreases ROS frequency due to snow cover depletion in early autumn and late spring (Figure 2). However, for the rest of the seasons and even with snow cover reductions, the snowpack does not fully disappear leading to ROS frequency increases due to more rainy days.

Con formato: Inglés (Estados Unidos)

Con formato: Inglés (Estados Unidos)

~~In detail,~~ SW and NW annual ROS frequency almost doubles (17 and 12 days/year, respectively) the one recorded in SE and NE (9 days/year, for both sectors). Maximum ROS frequency for a season ~~are~~is found in SW and NW because of larger snowpacks ~~magnitudes~~ in this sector (i.e., López-Moreno, 2005; López-Moreno et al, 2007; Navarro-Serrano et al., 2017; Bonsoms et al., 2021a). Thus, snow cover last longer until spring when minimum Sf values are found (Figure 2~~S1~~). SW and NW~~This~~ sectors ~~are~~is the most exposed to SW and W air flows (negative NAO phases) (López-Moreno, 2005), which bring wet and mild conditions over the mountain range, leading to most ROS-related floods in the range (Morán-Tejeda et al., 2019). ~~The generally ROS rainfall amount increase reported in this work (independently of the increment of temperature and~~

Con formato: Inglés (Estados Unidos)

Con formato: Inglés (Estados Unidos)

Con formato: Inglés (Estados Unidos)

Con formato: Inglés (Estados Unidos)

Con formato: Inglés (Estados Unidos)

~~elevation) is explained by the Sf reduction expected for all sectors (Figure 3).~~ Maximum ROS rainfall amount is generally detected in ~~spring (May),~~May, except in NE (at 2400 m elevation) ~~zones~~ and SE (all elevations). In the latter sectors, ROS rainfall amount tends to ~~dissapear~~disappear in Octuber under large (> 2ºC) increments of temperature. The seasonal snow accumulation in NE and SE is lower-than-average due to the lower influence of Atlantic climate in these sectors of the range. ~~Hence, large increments of warming decreases ROS frequency due to snow cover depletion in early autumn and late spring (Figure S1).~~ In addition, the SE is closer to the 0ºC due to higher-than-average sublimation, latent and radiative heat fluxes (Bonsoms et al., 2022) and for this reason in this sector each increment of temperature has larger effects on the Sf, HS and ROS frequency reduction (Figure 3). 2400 m elevation shows the largest variation over the ~~baseline climate~~historical climate period as well as ROS ~~exposure~~ rainfall amount and frequency (Figure 8) because of the larger snowpack ~~magnitude~~ and duration compared to 1500 m and 1800 m areas. Thus, 2400 m elevation snow duration last until spring and summer, when the largest shift from snowfall to rainfall is found. On the other hand, 1800 m elevation shows the maximum ROS rainfall amount since the amount of moisture for condensation decreases while air masses increase height (Roe and Baker, 2006). ~~Furthermore, The largest~~The largest ROS rainfall amount is detected in SE during autumn (Figure 7). ~~,~~ This sector is ~~because of the exposure of this region~~exposed to Mediterranean low-pressure systems (negative WeMO phases), that usually trigger heavy rainfall events (Lemus-Canovas et al., 2021) during this season, when snow cover may have already developed at sufficiently high elevation. ~~(Lemus-Canovas et al., 2021).~~

5.2 ROS ~~temporal evolution~~comparison with other studies

Recent ROS trends in other mid-latitude areas are in accordance with ROS analysis presented here. Freudiger et al. (2013) analyzed the ROS trends (1950 – 2011 period) of the Rhine, Danube, Elbe, Weser, Oder, and Ems (Central Europe) basins. They found an overall ROS frequency ~~increaase~~increase during January and February (1990 to 2011 period), which is consistent with the ROS rainfall amount and frequency increase ~~detected~~ simulated in winter for the Pyrenees for all elevations and increment of temperature. Similarly, in Sitter River (NE Switzerland), a ROS frequency increase of around 40% (200%) at <1500 m (>2500 m) was detected between 1960 and 2015 (Beniston and Stoffel, 2016). During the last half of the 20th century, ROS frequency trends show an upward (downward) trend in high (low) elevation in western United-States (McCabe et al., 2007), as well as in southern British Columbia (Loukas et al., 2002) and at catchment scale in Oregon (United-States) (Surfleet and Tullos, 2013). Same ROS frequency increases (decreases) has been detected from 1980 to 2010 in Norwegian at high (low) elevated mountain zones (Pall et al., 2019). However, in contradiction with our results and previous studies, winter Northern-Hemisphere ROS frequency trends (1979-2014 period) show no-clear trends (Cohen et al., 2015).

Results exposed in this work provide more evidence of ROS frequency increases in high-elevation zones, as it has been suggested by climate projections and ROS sensitivity to temperature studies. ROS shows an elevation-dependent pattern that was previously reported in the Swiss Alps (Morán-Tejeda et al., 2016). In

Sitter River (NE Switzerland), an increase of 2 to 4 °C over the 1960 to 2015 period results in an increase of the ROS frequency by around 50% at > 2500 m (Beniston and Stoffel, 2016). Likewise, 21st century high-emission scenarios (RCP8.5), suggest increases in ROS frequency and intensity in Gletsch (Switzerland) high-elevation area.~~; however, o~~Other studies suggest that on~~n~~ climate projections for ROS definitions that include snow melting (Musselman et al., 2018), natural climate variability contributes to a large extend (70 %) of ROS variability (Schirmer et al., 2022). Li et al. (2019) analyzed the future ROS frequency in the conterminous United-States and detected a nonlinear trend ROS due to warming, which is consistent with the different ROS rainfall amount and frequency responses depending on the increment of temperature detected in our work. Climate projections for the mid-end of the 21th century projected positive ROS frequency and rainfall trends in Western United-States and Canada (il Jeong and Sushama, 2018). Similarly, ROS frequency will likely decrease (increase) in the warmest months of the season in low (high) elevation areas of western United-States (Musselman et al., 2018). The same is projected Norwegian mountains (Mooney and Li, 2021). López-Moreno et al. (2021) analyzed 40 worldwide basins ROS sensitivity to warming. In their study they found a decrease of ROS events in warm mountain areas. However, they detected ROS frequency increases in cold-climate mountains where large snow accumulation is found despite warming. In accordance with our results, they identified large seasonal differences and ROS frequency decreases in Mediterranean mountains due to snow cover depletion in the lasts months of the snow season.

5.3 ROS ablation

Warming increases ROS ablation from autumn to winter on deep snowpacks and in the coldest sectors of the range, due to higher energy for snow ablation and closer 0ºC isotherm conditions in a warmer than ~~baseline climate~~the historical climate period. ~~Nevertheless, D~~Data show ~~1500 m~~no-changes and~~or~~ decreases in ROS ablation in SE and ~~spring, since~~spring since the snowpack is already near to the isothermal conditions. These results go in line with results ~~modelled~~ observed for cold and warm Pyrenean sites (López-Moreno et al., 2013) as well as for different Northern-Hemisphere sites (Essery et al., 2020). ROS ablation indicator is also indirectly affected by the HS magnitude decreases (30 % per ºC; Figure 3), and therefore lower ROS ablation is ~~direclty~~directly affected by lower HS magnitudes. Previous literature pointed out that warming have different ~~counter intuitive~~ effects on snow ablation patterns. Higher than average temperatures advance the peak HS date on average 5 days per ºC in 1800 m and 2400 m elevations (Bonsoms et al., 2023~~2b~~), triggering earlier snow ablation onsets, and therefore lower solar radiation fluxes (López-Moreno et al., 2013; Lundquist et al., 2013; Pomeroy et al., 2015; Musselman et al., 2017a; Sanmiguel-Vallelado et al., 2022), as well as earlier snow depletion before the maximum advection of heat fluxes into the snowpack (spring) (Bonsoms et al., 2022). Slower snow melt rates in a warmer climate have been detected in Western United-States (Musselman et al., 2017), as well as the entire Northern-Hemisphere (Wu et al., 2018). ~~1500 m~~Low or inexistent changes in snow ablation on warm and marginal snowpacks has been previously detected in the central Pyrenees (López-

Con formato: Inglés (Estados Unidos)

Con formato: Inglés (Estados Unidos)
Con formato: Inglés (Estados Unidos)
Con formato: Inglés (Estados Unidos)
Con formato: Inglés (Estados Unidos)
Con formato: Inglés (Estados Unidos)
Con formato: Inglés (Estados Unidos)
Con formato: Inglés (Estados Unidos)
Con formato: Inglés (Estados Unidos)
Con formato: Inglés (Estados Unidos)
Con formato: Inglés (Estados Unidos)
Con formato: Inglés (Estados Unidos)
Con formato: Inglés (Estados Unidos)
Con formato: Inglés (Estados Unidos)

Moreno et al., 2013), in forest and open areas (Sanmiguel-Valellado et al., 2022), in the entire range (Bonsoms et al., 2022), and other Iberian Peninsula Mountain ranges outside the Pyrenees (Alonso-González et al., 2020a).

ROS ablation is larger than the average snow ablation during a snow ablation day (Figure S5~~6~~) due to higher SEB positive fluxes. Several works analyzed SEB changes on ROS events, and different SEB contributions has been found depending on the geographical area (Mazurkiewicz et al., 2008; Garvelmann et al., 2014b; Würzer et al., 2016; Corripio and López-Moreno, 2017; Li et al., 2019), ranging from net radiation in Pacific North West (Mazurkiewick et al., 2008) to LW~~w~~in and turbulent heat fluxes in conterminous United-States mountain areas (Li et al., 2019) or the Swiss Alps (e.g., Würzer et al., 2016). In general, studies in mid-latitude mountain ranges have shown that turbulent heat fluxes contribute between 60 and 90 % of the energy available for snow ablation during ROS days (e.g., Marks et al., 1998; Garvelmann et al. 2014; Corripio and López-Moreno, 2017). In the central Pyrenees (at > 2000 m) the meteorological analysis of a ROS event reveals that ROS ablation is larger than a normal ablation day because of the large advection of LW~~w~~in and especially sensible heat fluxes (Corripio and López-Moreno, 2017). LW~~w~~in increases due to the high cloud cover and warm air, as it is frequently observed during ROS episodes (Moore and Owens, 1984). Further works should analyze the SEB controls during ROS events within the entire mountain range, as well as the ROS hydrological responses to climate warming.

5.4 ROS socio-environmental impacts and hazards

Temperature-induced changes in the seasonal snowpack and during ROS days suggest several hydrological shifts including, but not limited to, earlier peak flows on the season (Surfleet and Tullos, 2013), rapid streamflow peaks during high precipitation events in frozen soils (Shanley and Chalmers, 1999), faster soil moisture depletion and lower river discharges in spring due to earlier snow melt in the season (Stewart, 2009). The shortening of the snow season due to warming reported in this work will potentially alter alpine phenological patterns (i.e., Wipf and Rixen, 2010) and expand forest cover (Szczypta et al., 2015). Although ~~vegation~~vegetation branches intercept a large amount of snowfall, intermediate and high vegetation shields short-wave radiation, reduces snow wind-transport and turbulent heat fluxes (López-Moreno and Latron, 2008; Sanmiguel-Valellado et al., 2022). Snow-forest interactions, their sensitivity to climate change as well as the ROS hydrological response within a changing ~~landcape~~landscape is far from understood across the range and should be the base of ~~forecoming~~forthcoming works.

The higher ROS ~~exposure~~ rainfall amount and frequency (Figure 8) will likely imply an increase of ROS-related hazards and impacts in the mountain ecosystem. Heavy ROS rainfall amount changes snow ~~methamorphism~~metamorphism on saturated snowpacks and leads to high-speed water percolation (Singh et al., 1997). The subsequent water refreezing changes the snowpack conditions and creates an ice-layer in the snowpack that can reach the surface (Rennert et al., 2009). ROS can cause plant damage (Bjerke et al., 2017)

Con formato: Inglés (Estados Unidos)
Con formato: Inglés (Estados Unidos)
Con formato: Inglés (Estados Unidos)
Con formato: Inglés (Estados Unidos)
Con formato: Inglés (Estados Unidos)
Con formato: Inglés (Estados Unidos)
Con formato: Inglés (Estados Unidos)
Con formato: Inglés (Estados Unidos)
Con formato: Inglés (Estados Unidos)
Con formato: Inglés (Estados Unidos)
Con formato: Inglés (Estados Unidos)
Con formato: Inglés (Estados Unidos)
Con formato: Inglés (Estados Unidos)
Con formato: Inglés (Estados Unidos)
Con formato: Inglés (Estados Unidos)
Con formato: Inglés (Estados Unidos)
Con formato: Inglés (Estados Unidos)

and the ice encapsulation of vegetation in tundra ecosystems can trigger severe wildlife impacts, such as vertebrate herbivores starvation, ~~(Hansen et al 2013),~~ reindeer population mortality (Kohler and Aanes, 2004) and higher competition between species (Hansen et al 2014). Nevertheless, any study to the date analyzed ROS-related impacts in flora and fauna across Southern-European mountains. Snow albedo decay due positive heat fluxes and rainfall in ROS events (Corripio and López-Moreno, 2017), lead to faster snow ablation even on the next days (e.g., Singh et al. 1997). The combination of changes in internal snowpack processes, larger ROS rainfall amount, and more energy to ablate snow during spring could enhance snow runoff, especially during warm and wet snowpack conditions (Würzer et al., 2016). In snow-dominated regions ROS can lead to a specific type of avalanching (Conway and Raymond, 1993) and floods (Surfleet and Tullos, 2013). The latter are the most environmental damaging risk in Spain (Llasat et al., 2014) and around 50% of the flood in the Iberian Peninsula are due to ROS events (Morán-Tejeda et al., 2019). More than half of the historical (1940 to 2012) flood events in the Ésera river catchment (central Pyrenees) occurred during spring (Serrano-Notivoli et al., 2017), which coincides with the snow ablation season. ROS floods have also economic impacts. For instance, a ROS flood event that occurred on 13th June of 2013 in the Garonne River (Val d'Aran, central Pyrenees) cost approximately 20 million of euros to the public insurance (Llasat et al., 2014).

5.5 Limitations

This study evaluates the sensitivity of ROS responses to climate change, enabling a better understanding of the non-linear ROS spatiotemporal variations in different sectors and elevations of the Pyrenees. Instead of presenting diverse outputs from climate model ensembles (López-Moreno et al., 2010), we provide ROS sensitivity values per 1ºC, making them comparable to other regions and seasons. The temperature and precipitation change values used in this sensitivity analysis are based on established climate projections for the region (Amblar-Francés et al., 2020). ~~However,~~ P~~p~~recipitation projections in the Pyrenees, however, exhibit high uncertainties among different models, ~~GHGs~~ emission scenarios, and temporal periods (López-Moreno et al., 2008).

The SAFRAN meteorological system used in this work relies on a topographical spatial division and exhibit and accuracy of around 1 ºC in air temperature~~Ta~~ and around 20 mm in the monthly cumulative precipitation (Vernay et al., 2022). Precipitation phase partitioning methods are subject to uncertainties under close-to-isothermal conditions (Harder and Pomeroy, ~~et al.,~~ 2014~~0~~). Hydrological models are also subject to errors in the snowpack prediction (Essery, 2015). However, the FSM2 is a multiphysics snowpack model that has been validated previously in the Pyrenees (Bonsoms et al., 2023) and compared against different snowpack models (Krinner et al., 2018), providing evidence of its robustness.

6 Conclusions

The expected decreases in snowfall fraction (Sf) and height of snow (HS) due to climate warming will likely change ROS spatio-temporal patterns across the Pyrenees. Therefore, a better understanding of ROS is required. This work analyzed the ROS sensitivity to warming by forcing a physically based snow model with perturbed reanalysis climate data (~~1980-2019~~1980 – 2019 period) for 1500 m, 1800 m and 2400 m elevation areas of the Pyrenees. ROS sensitivity to temperature and precipitation is evaluated by frequency, rainfall intensity and snow ablation during ROS days.

Con formato: Inglés (Estados Unidos)

During the ~~baseline climate period~~historical climate period, annual ROS frequency totals on average 10, 12 and 10 day/season for 1500 m, 1800 m and 2400 m elevations. Higher-than-average annual ROS frequency are found in 1800 m elevation SW (17 days/year) and NW (12 days/year), which contrast with the minimums detected in SE (9 days/year). The different spatial and seasonal ROS response to warming suggest that contrasting and shifting trends could be expected in the future. Overall ROS frequency decreases during summer at~~in~~ 2400 m elevation for > 1ºC. When temperature is progressively increased the greatest ROS frequency increases are found for SW 2400 m elevation (around 1 day/month for + 1ºC). ROS frequency is ~~highlty~~highly sensitive to warming in the snow onset and offset ~~months, when~~months when ~~counterintuitive~~ diverging factors play a key role. On the one hand, maximum Sf decreases are ~~modeled~~simulated for spring, leading to rainfall increases; on the other hand, warming depletes the snowpack in the warmest and snow driest sectors of the range. Consequently, data suggest a general ROS frequency decrease for ~~the majority of~~most of the SE massifs, where the snowpack is near the isothermal conditions in the ~~baseline climate period~~historical climate period. Yet, during spring, the highest ROS frequency increases are detected in SW and NW, since these sectors are less exposed to radiative and turbulent heat fluxes and record higher-than-average seasonal snow accumulations.

Con formato: Inglés (Estados Unidos)

Con formato: Inglés (Estados Unidos)

Con formato: Inglés (Estados Unidos)

Con formato: Inglés (Estados Unidos)

Con formato: Inglés (Estados Unidos)

Con formato: Inglés (Estados Unidos)

Con formato: Inglés (Estados Unidos)

ROS rainfall amount generally increases due to warming, independently of the sector and elevation, being limited by the number of ROS days. The largest and constant increments are observed in spring, when ROS rainfall amount increases at a rate of 7, 6 and 3 % per ºC for 1500 m, 1800 m and ~~high~~2400 m, respectively. ROS rainfall amount increases ~~are explained~~is influenced by Sf reductions, which decrease at a rate of 29 %, 22 %, and 12 % per ºC for 1500 m, 1800 m, and 2400 m elevations, respectively. ROS rainfall amount maximum values are detected in SE (28 mm/day), especially in 1800 m elevation during autumn (45 mm/day), since this sector is exposed to subtropical Mediterranean flows.

Con formato: Inglés (Estados Unidos)

Con formato: Inglés (Estados Unidos)

Finally, ROS ablation shows contrasting patterns depending on the season, sector and elevation. Generally, ROS ablation increases in cold snowpacks, such as those ~~modeled~~simulated in 2400 m elevation and during cold seasons (autumn and winter). Here, ROS ablation follows a constant ablation rate of around + 10% per ºC, due to higher-than-average positive sensible and LWin heat fluxes. However, in SE and 1500 m elevation, where marginal and isothermal snowpacks are found, no changes or decreases in ROS ablation are detected due to snowpack ~~magnitude~~ reductions in a warmer climate. Results demonstrate the high snow sensitivity to climate within a mid-latitude mountain ~~range, and~~range and suggest significant changes with regards to water resources management. Relevant implications in the ecosystem and socio-economic activities associated with snow cover are anticipated.

Con formato: Inglés (Estados Unidos)

Con formato: Inglés (Estados Unidos)

Data availability

FSM2 is an open access snow model (Essery, 2015) provided at https://github.com/RichardEssery/FSM2 (last access 15 January 2023). SAFRAN climate dataset (Vernay et al., 2022) is available by AERIS at https://www.aeris-data.fr/landing-page/?uuid=865730e8-edeb-4c6b-ae58-80f95166509b#v2020.2 (last access 16 December 2022). Data of this work is available upon request by the first author (josepbonsoms5@ub.edu).

Author contribution

J.B., J.I.L.M., and E.A.G. designed the work. J.B. analyzed the data and wrote the manuscript. J.B., J.I.L.M., E.A.G., C.D.B., and M.O. provided feedback and edited the manuscript. J.I.L.M., M.O. supervised the project and acquired funding.

Competing interests

The authors declare that they have no conflict of interest.

Acknowledgements

This work frames within the research topics examined by the research group "Antarctic, Artic, Alpine Environments-ANTALP" (2017-SGR-1102) funded by the Government of Catalonia, HIDROIBERNIEVE (CGL2017-82216-R) and MARGISNOW (PID2021-124220OB-100), from the Spanish Ministry of Science, Innovation and Universities. JB is supported by a pre–doctoral University Professor FPI grant (PRE2021-097046) funded by the Spanish Ministry of Science, Innovation and Universities. The authors are grateful to Pascal Haegeli, Samuel Morin and an anonymous reviewer for their review of this manuscript.

References

Alonso-González, E., Aalstad, K., Baba, M. W., Revuelto, J., López-Moreno, J. I., Fiddes, J., et al. MuSA: The Multiscale Snow Data Assimilation System (v1.0). Geoscientific Model Development Discussions, 1–43. https://doi.org/10.5194/gmd-2022-137, 2022.

Alonso-González, E., López-Moreno, J.I., Navarro-Serrano, F., Sanmiguel-Vallelado, A., Aznárez-Balta, M., Revuelto, J., and Ceballos, A.: Snowpack Sensitivity to Temperature, Precipitation, and Solar Radiation Variability over an Elevational Gradient in the Iberian Mountains, Atmos. Res., 243, 104973 https://doi.org/10.1016/j.atmosres.2020.104973, 2020a.

Alonso-González, E., López-Moreno, J.I., Navarro-Serrano, F., Sanmiguel-Vallelado, A., Revuelto, J., Domínguez-Castro, F., and Ceballos, A.: Snow climatology for the mountains in the Iberian Peninsula using satellite imagery and simulations with dynamically downscaled reanalysis data, International Journal of Climatology, 40(1), 477–491, https://doi.org/10.1002/joc.6223, 2019.

Alonso-González, E., López-Moreno, J. I., Navarro-Serrano, F. M., and Revuelto, J.: Impact of North Atlantic Oscillation on the snowpack in Iberian Peninsula mountains, Water (Switzerland), 12, https://doi.org/10.3390/w12010105, 2020b.

Amblar-Francés, M. P., Ramos-Calzado, P., Sanchis-Lladó, J., Hernanz-Lázaro, A., Peral-García, M. C., Navascués, B., Dominguez-Alonso, M., Pastor-Saavedra, M. A., and Rodríguez-Camino, E.: High resolution climate change projections for the Pyrenees region, in: Advances in Science and Research, 191–208, https://doi.org/10.5194/asr-17-191-2020, 2020.

Barnett, T.P., Adam, J.C., and Lettenmaier, D.P., Potential impacts of a warming climate on water availability in snow-dominated regions. Nature. https://doi.org/10.1038/nature04141 2005.

Bartsch, A., Kumpula, T., Forbes, B. C., and Stammler, F.: Detection of snow surface thawing and refreezing in the Eurasian arctic with QuikSCAT: Implications for reindeer herding, Ecological Applications, 20, 2346–2358, https://doi.org/10.1890/09-1927.1, 2010.

Beniston, M. and Stoffel, M.: Rain-on-snow events, floods and climate change in the Alps: Events may increase with warming up to 4 °C and decrease thereafter, Science of the Total Environment, 571, 228–236, https://doi.org/10.1016/j.scitotenv.2016.07.146, 2016.

Beniston, M., Farinotti, D., Stoffel, M., Andreassen, L. M., Coppola, E., Eckert, N., Fantini, A., Giacona, F., Hauck, C., Huss, M., Huwald, H., Lehning, M., López-Moreno, J. I., Magnusson, J., Marty, C., Morán-Tejéda, E., Morin, S., Naaim, M., Provenzale, A., Rabatel, A., Six, D., Stötter, J., Strasser, U., Terzago, S., and Vincent, C.: The European mountain cryosphere: A review of its current state, trends, and future challenges, https://doi.org/10.5194/tc-12-759-2018, 2018.

Bieniek, P. A., Bhatt, U. S., Walsh, J. E., Lader, R., Griffith, B., Roach, J. K., and Thoman, R. L.: Assessment of Alaska rain-on-snow events using dynamical downscaling, J Appl Meteorol Climatol, 57, 1847–1863, https://doi.org/10.1175/JAMC-D-17-0276.1, 2018.

Bintanja, R. and Andry, O.: Towards a rain-dominated Arctic, Nat Clim Chang, 7, 263–267, https://doi.org/10.1038/nclimate3240, 2017.

Bonsoms, J., Franch, F. S., and Oliva, M.: Snowfall and snow cover evolution in the eastern pre-pyrenees (Ne iberian peninsula), Geographical Research Letters, 47, 291–307, https://doi.org/10.18172/cig.4879, 2021a.

Bonsoms, J., González, S., Prohom, M., Esteban, P., Salvador-Franch, F., López-Moreno, J. I., and Oliva, M.: Spatio-temporal patterns of snow in the Catalan Pyrenees (NE Iberia), International Journal of Climatology, 41, 5676–5697, https://doi.org/10.1002/joc.7147, 2021b.

Bonsoms, J., López-Moreno, J. I., González, S., and Oliva, M.: Increase of the energy available for snow ablation in the Pyrenees (1959–2020) and its relation to atmospheric circulation, Atmos Res, 275, https://doi.org/10.1016/j.atmosres.2022.106228, 2022a.

Bonsoms, J., López-Moreno, J. I., and Alonso-González, E.: Snow sensitivity to temperature and precipitation change during compound cold–hot and wet–dry seasons in the Pyrenees, The Cryosphere, 17, 1307–1326, https://doi.org/10.5194/tc-17-1307-2023, 2023.

Buisan, S.T., López-Moreno, J.I., Sanz, M.A. and Korchendorfer, J. Impact of weather type variability on winter precipitation, temperature and annual snowpack in the Spanish Pyrenees. Climate Research, 69, 79–92. https://doi.org/10.3354/cr01391, 2016.

Bjerke JW, Treharne R, Vikhamar-Schuler D, Karlsen S R, Ravolainen V, Bokhorst S, Phoenix G K, Bochenek

Con formato: Inglés (Estados Unidos)

Con formato: Inglés (Estados Unidos)

Con formato: Inglés (Estados Unidos)

Con formato: Inglés (Estados Unidos)

Z and Tømmervik H 2017 Understanding the drivers of extensive plant damage in boreal and Arctic ecosystems: insights from field surveys in the aftermath of damage Sci. Total Environ. 599 1965–76.

Céron, J. P., Tanguy, G., Franchistéguy, L., Martin, E., Regimbeau, F., and Vidal, J. P.: Hydrological seasonal forecast over France: Feasibility and prospects, Atmospheric Science Letters, 11, 78–82, https://doi.org/10.1002/asl.256, 2010.

Cohen, J., Ye, H., and Jones, J.: Trends and variability in rain-on-snow events, Geophys Res Lett, 42, 7115–7122, https://doi.org/10.1002/2015GL065320, 2015.

Collados-Lara, A. J., Pulido-Velazquez, D., Pardo-Igúzquiza, E., and Alonso-González, E.: Estimation of the spatio-temporal dynamic of snow water equivalent at mountain range scale under data scarcity, Science of the Total Environment, 741, https://doi.org/10.1016/j.scitotenv.2020.140485, 2020.

Conway, H. and Raymond, C. F.: Snow stability during rain, Journal of Glaciology, 39, 635–642, https://doi.org/10.3189/s0022143000016531, 1993.

Corripio, J. G. and López-Moreno, J. I.: Analysis and predictability of the hydrological response of mountain catchments to heavy rain on snow events: A case study in the Spanish Pyrenees, Hydrology, 4, https://doi.org/10.3390/hydrology4020020, 2017.

Crawford, A. D., Alley, K. E., Cooke, A. M., and Serreze, M. C.: Synoptic Climatology of Rain-on-Snow Events in Alaska, https://doi.org/10.1175/MWR-D-19, 2020.

Deschamps-Berger, C., Cluzet, B., Dumont, M., Lafaysse, M., Berthier, E., Fanise, P., and Gascoin, S.: Improving the Spatial Distribution of Snow Cover Simulations by Assimilation of Satellite Stereoscopic Imagery, Water Resour. Res., 58, e2021WR030271, https://doi.org/10.1029/2021WR030271, 2022.

Del Barrio, G., Creus, J., and Puigdefabregas, J.: Thermal Seasonality of the High Mountain Belts of the Pyrenees, Mt. Res. Dev., 10, 227–233, 1990.

Devers, A., Vidal, J. P., Lauvernet, C., and Vannier, O.: FYRE Climate: A high-resolution reanalysis of daily precipitation and temperature in France from 1871 to 2012, Climate of the Past, 17, 1857–1879, https://doi.org/10.5194/cp-17-1857-2021, 2021.

Durand, Y., Giraud, G., Brun, E., Mérindol, L., and Martin, E.: A computer-based system simulating snowpack structures as a tool for regional avalanche forecasting, Journal of Glaciology, 45, 469–484, https://doi.org/10.3189/s0022143000001337, 1999.

Durand, Y., Laternser, M., Giraud, G., Etchevers, P., Lesaffre, B., and Mérindol, L.: Reanalysis of 44 yr of climate in the French Alps (1958-2002): Methodology, model validation, climatology, and trends for air temperature and precipitation, J Appl Meteorol Climatol, 48, 429–449, https://doi.org/10.1175/2008JAMC1808.1, 2009.

Essery, R.: A factorial snowpack model (FSM 1.0), Geosci Model Dev, 8, 3867–3876, https://doi.org/10.5194/gmd-8-3867-2015, 2015.

Essery, R., Kim, H., Wang, L., Bartlett, P., Boone, A., Brutel-Vuilmet, C., Burke, E., Cuntz, M., Decharme, B., Dutra, E., Fang, X., Gusev, Y., Hagemann, S., Haverd, V., Kontu, A., Krinner, G., Lafaysse, M., Lejeune, Y., Marke, T., Marks, D., Marty, C., Menard, C. B., Nasonova, O., Nitta, T., Pomeroy, J., Schädler, G.,

Con formato: Inglés (Estados Unidos)

Con formato: Inglés (Estados Unidos)

Con formato: Inglés (Estados Unidos)

Semenov, V., Smirnova, T., Swenson, S., Turkov, D., Wever, N., and Yuan, H.: Snow cover duration trends observed at sites and predicted by multiple models, Cryosphere, 14, 4687–4698, https://doi.org/10.5194/tc-14-4687-2020, 2020.

Freudiger, D., Kohn, I., Stahl, K., and Weiler, M.: Large-scale analysis of changing frequencies of rain-on-snow events with flood-generation potential, Hydrol Earth Syst Sci, 18, 2695–2709, https://doi.org/10.5194/hess-18-2695-2014, 2014.

García-Ruiz, J. M., López-Moreno, J. I., Vicente-Serrano, S. M., Lasanta–Martínez, T. and Beguería, S. Mediterranean water resources in a global change scenario, Earth Sci. Rev., 105(3–4), 121–139, https://doi.org/10.1016/j.earscirev.2011.01.006, 2011.

Garvelmann, J., Pohl, S., and Weiler, M.: Variability of observed energy fluxes during rain-on-snow and clear sky snowmelt in a midlatitude mountain environment, J Hydrometeorol, 15, 1220–1237, https://doi.org/10.1175/JHM-D-13-0187.1, 2014.

Günther, D., Marke, T., Essery, R., and Strasser, U.: Uncertainties in Snowpack Simulations—Assessing the Impact of Model Structure, Parameter Choice, and Forcing Data Error on Point-Scale Energy Balance Snow Model Performance, Water Resour Res, 55, 2779–2800, https://doi.org/10.1029/2018WR023403, 2019.

Habets, F., Boone, A., Champeaux, J. L., Etchevers, P., Franchistéguy, L., Leblois, E., Ledoux, E., le Moigne, P., Martin, E., Morel, S., Noilhan, J., Seguí, P. Q., Rousset-Regimbeau, F., and Viennot, P.: The SAFRAN-ISBA-MODCOU hydrometeorological model applied over France, Journal of Geophysical Research Atmospheres, 113, https://doi.org/10.1029/2007JD008548, 2008.

~~Hansen, B.B., Grøtan, V., Aanes, R., et al., 2013. Climate events synchronize the dynamics of a resident vertebrate community in the High Arctic. Science 339, 313–315.~~

Hansen, B.B., Isaksen, K., Benestad, R.E., et al.~~, 2014~~. Warmer and wetter winters: characteristics and implications of an extreme weather event in the High Arctic. Environ. Res. Lett. 9, 114021.

Harder, P. and Pomeroy, J.: Hydrological model uncertainty due to precipitation-phase partitioning methods~~Estimating precipitation phase using a psychrometric energy balance method~~, Hydrological Processes, 28~~7(13)~~, 4311–4327~~1901–1914~~. https://doi.org/10.1002/hyp.9799, 2014.~~3~~

Immerzeel, W. W., Lutz, A. F., Andrade, M., Bahl, A., Biemans, H., Bolch, T., Hyde, S., Brumby, S., Davies, B. J., Elmore, A. C., Emmer, A., Feng, M., Fernández, A., Haritashya, U., Kargel, J. S., Koppes, M., Kraaijenbrink, P. D. A., Kulkarni, A. v., Mayewski, P. A., Nepal, S., Pacheco, P., Painter, T. H., Pellicciotti, F., Rajaram, H., Rupper, S., Sinisalo, A., Shrestha, A. B., Viviroli, D., Wada, Y., Xiao, C., Yao, T., and Baillie, J. E. M.: Importance and vulnerability of the world's water towers, Nature, 577, 364–369, https://doi.org/10.1038/s41586-019-1822-y, 2020.

IPCC: High Mountain Areas, in: The Ocean and Cryosphere in a Changing Climate, Cambridge University Press, 131–202, https://doi.org/10.1017/9781009157964.004, 2022.

Jennings, K. S., Winchell, T. S., Livneh, B., and Molotch, N. P.: Spatial variation of the rain-snow temperature threshold across the Northern Hemisphere, Nat Commun, 9, https://doi.org/10.1038/s41467-018-03629-7, 2018.

il Jeong, D. and Sushama, L.: Rain-on-snow events over North America based on two Canadian regional climate models, Clim Dyn, 50, 303–316, https://doi.org/10.1007/s00382-017-3609-x, 2018.

Kohler, J. and Aanes, R.: Effect of winter snow and ground-icing on a Svalbard reindeer population: Results of a simple snowpack model, in: Arctic, Antarctic, and Alpine Research, 333–341, https://doi.org/10.1657/1523-0430(2004)036[0333:EOWSAG]2.0.CO;2, 2004.

Krinner, G., Derksen, C., Essery, R., Flanner, M., Hagemann, S., Clark, M., Hall, A., Rott, H., Brutel-Vuilmet, C., Kim, H., Ménard, C. B., Mudryk, L., Thackeray, C., Wang, L., Arduini, G., Balsamo, G., Bartlett, P., Boike, J., Boone, A., Chéruy, F., Colin, J., Cuntz, M., Dai, Y., Decharme, B., Derry, J., Ducharne, A., Dutra, E., Fang, X., Fierz, C., Ghattas, J., Gusev, Y., Haverd, V., Kontu, A., Lafaysse, M., Law, R., Lawrence, D., Li, W., Marke, T., Marks, D., Ménégoz, M., Nasonova, O., Nitta, T., Niwano, M., Pomeroy, J., Raleigh, M. S., Schaedler, G., Semenov, V., Smirnova, T. G., Stacke, T., Strasser, U., Svenson, S., Turkov, D., Wang, T., Wever, N., Yuan, H., Zhou, W., and Zhu, D.: ESM-SnowMIP: assessing snow models and quantifying snow-related climate feedbacks, Geosci. Model Dev., 11, 5027–5049, https://doi.org/10.5194/gmd-11-5027-2018, 2018.

Lemus-Canovas, M., Lopez-Bustins, J. A., Trapero, L., and Martin-Vide, J.: Combining circulation weather types and daily precipitation modelling to derive climatic precipitation regions in the Pyrenees, Atmos Res, 220, 181–193, https://doi.org/10.1016/j.atmosres.2019.01.018, 2019.

Lemus-Canovas, M., Lopez-Bustins, J. A., Martín-Vide, J., Halifa-Marin, A., Insua-Costa, D., Martinez-Artigas, J., Trapero, L., Serrano-Notivoli, R., and Cuadrat, J. M.: Characterisation of extreme precipitation events in the Pyrenees: From the local to the synoptic scale, Atmosphere (Basel), 12, https://doi.org/10.3390/atmos12060665, 2021.

Li, D., Lettenmaier, D. P., Margulis, S. A., and Andreadis, K.: The Role of Rain-on-Snow in Flooding Over the Conterminous United States, Water Resour Res, 55, 8492–8513, https://doi.org/10.1029/2019WR024950, 2019.

Llasat, M. C., Marcos, R., Llasat-Botija, M., Gilabert, J., Turco, M., and Quintana-Seguí, P.: Flash flood evolution in North-Western Mediterranean, Atmos Res, 149, 230–243, https://doi.org/10.1016/j.atmosres.2014.05.024, 2014.

López-Moreno, J. I.: Recent variations of snowpack depth in the central Spanish Pyrenees, Arct Antarct Alp Res, 37, 253–260, https://doi.org/10.1657/1523-0430(2005)037[0253:RVOSDI]2.0.CO;2, 2005.

López-Moreno,J.I., Goyette,S., and Beniston,M.:Climate change prediction over complex areas: spatial variability of uncertainties and predictions over the Pyrenees from a set of regional climate models. International Journal of Climatology, 28, 1535–1550. https://doi.org/10.1002/joc.1645, 2008.

López-Moreno, J. I., Pomeroy, J. W., Revuelto, J., and Vicente-Serrano, S. M.: Response of snow processes to climate change: Spatial variability in a small basin in the Spanish Pyrenees, Hydrol Process, 27, 2637–2650, https://doi.org/10.1002/hyp.9408, 2013.

López-Moreno, J. I., Pomeroy, J. W., Morán-Tejeda, E., Revuelto, J., Navarro-Serrano, F. M., Vidaller, I., and Alonso-González, E.: Changes in the frequency of global high mountain rain-on-snow events due to climate warming, Environmental Research Letters, 16, https://doi.org/10.1088/1748-9326/ac0dde, 2021.

López-Moreno, J.I., Soubeyroux, J.M., Gascoin, S., Alonso-González, E., Durán-Gómez, N., Lafaysse, M., Vernay, M., Carmagnola, C. and Morin, S. Long-term trends (1958–2017) in snow cover duration and depth in the Pyrenees. International Journal of Climatology, 40, 1–15. https://doi.org/10.1002/joc.6571, 2020.

López-Moreno, J.I., and Vicente-Serrano, S.M.: Atmospheric circulation influence on the interannual

Con formato: Color de fuente: Automático

variability of snowpack in the Spanish Pyrenees during the second half of the twentieth century, Nord. Hydrol., 38 (1), 38–44, https://doi.org/10.2166/ nh.2007.030, 2007.

López-Moreno, J.I., and Latron, J., 2008. Spatial heterogeneity in snow water equivalent induced by forest canopy in a mixed beech-fir stand in the Pyrenees. Ann. Glaciol. 49 (1), 83–90, https://doi.org/10.3189/172756408787814951, 2008.

Loukas, A., Vasiliades, L., and Dalezios, N. R.: Potential climate change impacts on flood producing mechanisms in southern British Columbia, Canada using the CGCMA1 simulation results, J. Hydrol., 259, 163–188, https:// doi.org/10.1016/S0022- 1694(01)00580-7, 2002

Lundquist, J. D., Dickerson-Lange, S. E., Lutz, J. A., and Cristea, N. C.: Lower forest density enhances snow retention in regions with warmer winters: A global framework developed from plot-scale observations and modeling, Water Resour Res, 49, 6356–6370, https://doi.org/10.1002/wrcr.20504, 2013.

Lynn, E., Cuthbertson, A., He, M., Vasquez, J. P., Anderson, M. L., Coombe, P., Abatzoglou, J. T., and Hatchett, B. J.: Technical note: Precipitation-phase partitioning at landscape scales to regional scales, Hydrol Earth Syst Sci, 24, 5317–5328, https://doi.org/10.5194/hess-24-5317-2020, 2020.

Matiu, M., Crespi, A., Bertoldi, G., Carmagnola, C.M., Marty, C., Morin, S., Schöner, W.,Cat Berro, D., Chiogna, G., De Gregorio, L., Kotlarski, S., Majone, B., Resch, G., Terzago, S., Valt, M., Beozzo, W., Cianfarra, P., Gouttevin, I., Marcolini, G., Notarnicola, C., Petitta, M., Scherrer, S.C., Strasser, U., Winkler, M., Zebisch, M., Cicogna, A., Cremonini, R., Debernardi, A., Faletto, M., Gaddo, M., Giovannini, L., Mercalli, L., Soubeyroux, J.-M., Susnik, A., Trenti, A., Urbani, S., Weilguni, V. Observed snow depth trends in the European Alps 1971 to 2019. Cryophere, 1–50. https://doi.org/10.5194/tc-2020-289, 2020.

Marks, D., Link, T., Winstral, A., and Garen, D.: Simulating snowmelt processes during rain-on-snow over a semi-arid mountain basin, 1992.

Martin, E., Brun, E., and Durand, Y.: Sensitivity of the French Alps snow cover to the variation of climatic variables, Annales Geophysicae, 12, 469–477, 1994.

Marty, C., Schlögl, S., Bavay, M., and Lehning, M.: How much can we save? Impact of different emission scenarios on future snow cover in the Alps, Cryosphere, 11, 517–529, https://doi.org/10.5194/tc-11-517-2017, 2017.

Mazurkiewicz, A. B., Callery, D. G., and McDonnell, J. J.: Assessing the controls of the snow energy balance and water available for runoff in a rain-on-snow environment, J Hydrol (Amst), 354, 1–14, https://doi.org/10.1016/j.jhydrol.2007.12.027, 2008.

Mazzotti, G., Essery, R., Webster, C., Malle, J., and Jonas, T.: Process-Level Evaluation of a Hyper-Resolution Forest Snow Model Using Distributed Multisensor Observations, Water Resour Res, 56, https://doi.org/10.1029/2020WR027572, 2020.

Mccabe, G. J., Clark, M. P., and Hay, L. E.: Rain-on-snow events in the Western United-States, https://doi.org/10.1175/BAMS-88-3-3I9, 2007.

Mooney, P. A. and Li, L.: Near future changes to rain-on-snow events in Norway, Environmental Research Letters, 16, https://doi.org/10.1088/1748-9326/abfdeb, 2021.

Con formato: Izquierda, Espacio Antes: 0 pto, Interlineado: 1,5 líneas

Con formato: Fuente: Diseño: Claro (Color personalizado(RGB(252;252;252)))

Morán-Tejeda, E., López-Moreno, J. I., Stoffel, M., and Beniston, M.: Rain-on-snow events in Switzerland: Recent observations and projections for the 21st century, Clim Res, 71, 111–125, https://doi.org/10.3354/cr01435, 2016.

Morán-Tejeda, E., Fassnacht, S. R., Lorenzo-Lacruz, J., López-Moreno, J. I., García, C., Alonso-González, E., and Collados-Lara, A. J.: Hydro-meteorological characterization of major floods in Spanish mountain rivers, Water (Switzerland), 11, https://doi.org/10.3390/W11122641, 2019.

Morin, S., Horton, S., Techel, F., Bavay, M., Coléou, C., Fierz, C., Gobiet, A., Hagenmuller, P., Lafaysse, M., Ližar, M., Mitterer, C., Monti, F., Müller, K., Olefs, M., Snook, J. S., van Herwijnen, A., and Vionnet, V.: Application of physical snowpack models in support of operational avalanche hazard forecasting: A status report on current implementations and prospects for the future, https://doi.org/10.1016/j.coldregions.2019.102910, 2020.

Musselman, K. N., Clark, M. P., Liu, C., Ikeda, K., and Rasmussen, R.: Slower snowmelt in a warmer world, Nat Clim Chang, 7, 214–219, https://doi.org/10.1038/nclimate3225, 2017a.

Musselman, K. N., Keitholotch, N. P., Mar, N., and Mgulis, S. A.: Snowmelt response to simulated warming across a large elevation gradient, southern sierra Nevada, California, Cryosphere, 11, 2847–2866, https://doi.org/10.5194/tc-11-2847-2017, 2017b.

Musselman, K. N., Lehner, F., Ikeda, K., Clark, M. P., Prein, A. F., Liu, C., Barlage, M., and Rasmussen, R.: Projected increases and shifts in rain-on-snow flood risk over western North America, https://doi.org/10.1038/s41558-018-0236-4, 2018.

Navarro-Serrano, F. and López-Moreno, J. I.: Análisis espacio-temporal de los eventos de nevadas en el pirineo Español y su relación con la circulación atmosférica, Cuadernos de Investigacion Geografica, 43, 233–254, https://doi.org/10.18172/cig.3042, 2017.

Ohba, M. and Kawase, H.: Rain-on-Snow events in Japan as projected by a large ensemble of regional climate simulations, Clim Dyn, 55, 2785–2800, https://doi.org/10.1007/s00382-020-05419-8, 2020.

OPCC-CTP. Climate change in the Pyrenees: Impacts, vulnerabilities and adaptation bases of knowledge for the future climate change adaptation strategy in the Pyrenees. 2018. 147. Jaca, Spain. https://www.opccctp.org/sites/default/files/editor/ opcc-informe-en-paginas.pdf. (last acces December 25, 2022)

Con formato: Inglés (Estados Unidos)

Pall, P., Tallaksen, L. M., and Stordal, F.: A Climatology of Rain-on-Snow Events for Norway, https://doi.org/10.1175/JCLI-D-18, 2019.

Pepin, N. C., Arnone, E., Gobiet, A., Haslinger, K., Kotlarski, S., Notarnicola, C., Palazzi, E., Seibert, P., Serafin, S., Schöner, W., Terzago, S., Thornton, J. M., Vuille, M., and Adler, C.: Climate Changes and Their Elevational Patterns in the Mountains of the World, https://doi.org/10.1029/2020RG000730, 2022.

Peña-Angulo, D., Vicente-Serrano, S., Domínguez-Castro, F., Murphy, C., Reig, F., Tramblay, Y., Trigo, R., Luna, M.Y., Turco, M., Noguera, I., Aznarez-Balta, M., Garcia-Herrera, R., Tomas-Burguera, M. and Kenawy, A. Long-term precipitation in Southwestern Europe reveals no clear trend attributable to anthropogenic forcing. Environmental Research Letters,15. 094070https://doi.org/10.1088/1748-9326/ab9c4f, 2020.

Pons,M., López-Moreno, J., Rosas-Casals, M., and Jover, E.: The vulnerability of Pyrenean ski resorts to climate-induced changes in the snowpack, Clim.Change, 131, 591–605, https://doi.org/10.1007/s10584-015-

1400-8, 2015.

Pomeroy, J. W., Fang, X., and Rasouli, K.: Sensitivity of snow processes to warming in the Canadian Rockies, 2015.

Pomeroy, J. W., Fang, X., and Marks, D. G.: The cold rain-on-snow event of June 2013 in the Canadian Rockies — characteristics and diagnosis, Hydrol Process, 30, 2899–2914, https://doi.org/10.1002/hyp.10905, 2016.

Rasouli, K., Pomeroy, J. W., and Whitfield, P. H.: Hydrological responses of headwater basins to monthly perturbed climate in the North American Cordillera, J Hydrometeorol, 20, 863–882, https://doi.org/10.1175/JHM-D-18-0166.1, 2019.

Rennert, K. J., Roe, G., Putkonen, J., and Bitz, C. M.: Soil thermal and ecological impacts of rain on snow events in the circumpolar arctic, J Clim, 22, 2302–2315, https://doi.org/10.1175/2008JCLI2117.1, 2009.

Réveillet, M., Dumont, M., Gascoin, S., Lafaysse, M., Nabat, P., Ribes, A., Nheili, R., Tuzet, F., Ménégoz, M., Morin, S., Picard, G., and Ginoux, P.: Black carbon and dust alter the response of mountain snow cover under climate change, Nat Commun, 13, https://doi.org/10.1038/s41467-022-32501-y, 2022.

Revuelto, J., Lecourt, G., Lafaysse, M., Zin, I., Charrois, L., Vionnet, V., Dumont, M., Rabatel, A., Six, D., Condom, T., Morin, S., Viani, A., and Sirguey, P.: Multi-criteria evaluation of snowpack simulations in complex alpine terrain using satellite and in situ observations, Remote Sens (Basel), 10, https://doi.org/10.3390/rs10081171, 2018.

Roe, G. H. and Baker, M. B.: Microphysical and Geometrical Controls on the Pattern of Orographic Precipitation, 2006.

Sanmiguel-Vallelado, A., McPhee, J., Esmeralda Ojeda Carreño, P., Morán-Tejeda, E., Julio Camarero, J., and López-Moreno, J. I.: Sensitivity of forest–snow interactions to climate forcing: Local variability in a Pyrenean valley, J Hydrol (Amst), 605, https://doi.org/10.1016/j.jhydrol.2021.127311, 2022.

Schirmer, M., Winstral, A., Jonas, T., Burlando, P., and Peleg, N.: Natural climate variability is an important aspect of future projections of snow water resources and rain-on-snow events, Cryosphere, 16, 3469–3488, https://doi.org/10.5194/tc-16-3469-2022, 2022.

Schöner, W., Koch, R., Matulla, C., Marty, C., and Tilg, A. M.: Spatio-temporal patterns of snow depth within the Swiss-Austrian Alps for the past half century (1961 to 2012) and linkages to climate change, International Journal of Climatology, 39, 1589–1603, https://doi.org/10.1002/joc.5902, 2019.

Serrano-Notivoli, R., Buisan, S.T., Abad-Pérez, L.M., Sierra-Álvarez, E., Rodríguez-Ballesteros, C., López-Moreno, J.I. and Cuadrat, J.M. Tendencias recientes en precipitación, temperatura y nieve de alta montaña en los Pirineos (Refugio de Góriz, Huesca). In: El clima: aire, agua, tierra y fuego. Madrid, Spain: Asociación Española de Climatología y Ministerio para la Transición Ecológica – Agencia Estatal de Meteorología, pp. 267, 1060–280, 2018.

Serrano-Notivoli, R., Mora, D., Ollero, A., Sánchez-Fabre, M., Sanz, P., and Saz, M.: Floodplain occupation and flooding in the central Pyrenees, Cuadernos de Investigacion Geografica, 43, 309–328, https://doi.org/10.18172/cig.3057, 2017.

Serreze, M. C., Gustafson, J., Barrett, A. P., Druckenmiller, M. L., Fox, S., Voveris, J., Stroeve, J., Sheffield, B., Forbes, B. C., Rasmus, S., Laptander, R., Brook, M., Brubaker, M., Temte, J., McCrystall, M. R., and

Bartsch, A.: Arctic rain on snow events: Bridging observations to understand environmental and livelihood impacts, Environmental Research Letters, 16, https://doi.org/10.1088/1748-9326/ac269b, 2021.

Shanley, J. B. and Chalmers, A.: The efect of frozen soil on snowmelt runoff at Sleepers River, Vermont 1999.

Singh, P., Spitzbart, G., Hübl, H., and Weinmeister, H. W.: Hydrological response of snowpack under rain-on-snow events: a field study, Journal of Hydrology, 1–20 pp., 1997.
Smyth, E. J., Raleigh, M. S., and Small, E. E. (2020). Improving SWE estimation with data assimilation: The influence of snow depth observation timing and uncertainty. Water Resources Research, 56, e2019WR026853. https://doi.org/ 10.1029/2019WR026853

Spandre, P., François, H., Verfaillie, D., Lafaysse, M., Déqué, M., Eckert, N., George, E., and Morin, S.: Climate controls on snow reliability in French Alps ski resorts, Sci Rep, 9, https://doi.org/10.1038/s41598-019-44068-8, 2019.

Stewart, I. T.: Changes in snowpack and snowmelt runoff for key mountain regions, https://doi.org/10.1002/hyp.7128, 2009.

Surfleet, C. G. and Tullos, D.: Variability in effect of climate change on rain-on-snow peak flow events in a temperate climate, J Hydrol (Amst), 479, 24–34, https://doi.org/10.1016/j.jhydrol.2012.11.021, 2013.

Szczypta, C., Gascoin, S., Houet, T., Hagolle, O., Dejoux, J.-F., Vigneau, C., and Fanise, P.: Impact of climate and land cover changes on snow cover in a small Pyrenean catchment, J. Hydrol., 521, 84–99, doi:10.1016/j.jhydrol.2014.11.060, 2015.

Verfaillie, D., Lafaysse, M., Déqué, M., Eckert, N., Lejeune, Y., and Morin, S.: Multi-component ensembles of future meteorological and natural snow conditions for 1500 m altitude in the Chartreuse mountain range, Northern French Alps, Cryosphere, 12, 1249–1271, https://doi.org/10.5194/tc-12-1249-2018, 2018.

Vernay, M., Lafaysse, M., Monteiro, D., Hagenmuller, P., Nheili, R., Samacoïts, R., Verfaillie, D., and Morin, S.: The S2M meteorological and snow cover reanalysis over the French mountainous areas: description and evaluation (1958-2021), Earth Syst Sci Data, 14, 1707–1733, https://doi.org/10.5194/essd-14-1707-2022, 2022.

Vicente-Serrano, S.M., Rodríguez-Camino, E., Domínguez-Castro, F., El Kenawy, A., Azorín-Molina, C. An updated review on recent trends in observational surface atmospheric variables and their extremes over Spain. Cuadernos de Investigación Geográfica (Geographical Research Letters) 43 (1), 209-232. https://doi.org/10.18172/cig.3134, 2017.

Vidaller, I., Revuelto, J., Izagirre, E., Rojas-Heredia, F., Alonso-González, E., Gascoin, S., René, P., Berthier, E., Rico, I., Moreno, A., Serrano, E., Serreta, A., López-Moreno, J.I. Toward an ice-free mountain range: Demise of Pyrenean glaciers during 2011–2020. J. Geophys. Res. Lett. 48, e2021GL094339 https://doi.org/10.1029/2021GL094339, 2021.

Viviroli, D., Archer, D. R., Buytaert, W., Fowler, H. J., Greenwood, G. B., Hamlet, A. F., Huang, Y., Koboltschnig, G., Litaor, M. I., López-Moreno, J. I., Lorentz, S., Schädler, B., Schreier, H., Schwaiger, K., Vuille, M., and Woods, R.: Climate change and mountain water resources: Overview and recommendations for research, management and policy, Hydrol Earth Syst Sci, 15, 471–504, https://doi.org/10.5194/hess-15-471-2011, 2011.

Westermann, S., Boike, J., Langer, M., Schuler, T. V., and Etzelmüller, B.: Modeling the impact of wintertime

Con formato: Inglés (Estados Unidos)

rain events on the thermal regime of permafrost, Cryosphere, 5, 945–959, https://doi.org/10.5194/tc-5-945-2011, 2011.

Wipf, S. and Rixen, C.: A review of snow manipulation experiments in Arctic and alpine tundra ecosystems, https://doi.org/10.1111/j.1751-8369.2010.00153.x, 2010.

Wu, X., Che, T., Li, X., Wang, N., and Yang, X.: Slower Snowmelt in Spring Along With Climate Warming Across the Northern Hemisphere, Geophys Res Lett, 45, 12,331-12,339, https://doi.org/10.1029/2018GL079511, 2018.

Würzer, S., Jonas, T., Wever, N., and Lehning, M.: Influence of initial snowpack properties on runoffformation during rain-on-snow events, J Hydrometeorol, 17, 1801–1815, https://doi.org/10.1175/JHM-D-15-0181.1, 2016.